U.PORTO

FEUP FACULDADE DE ENGENHARIA
UNIVERSIDADE DO PORTO

INTEGRATED MASTER IN ENVIRONMENTAL ENGINEERING 2017/2018

Advances in bromate reduction by heterogeneous TiO_2 photocatalysis: The use of a static mixer as photocatalyst support

Dissertation submitted in partial fulfillment of the requirements for the degree of Master of Science in Environmental Engineering at the Faculty of Engineering of University of Porto

DANIELA FILIPA SOUSA MORAIS

Developed in

Associate Laboratory LSRE-LCM – Laboratory of Separation and Reaction Engineering - Laboratory of Catalysis and Materials, Faculty of Engineering of University of Porto

SRE
CM

Supervisor: Maria Francisca da Costa Moreira, PhD
Post-doctoral Researcher in the Associate Laboratory LSRE-LCM

Co-Supervisor: Vítor Jorge Pais Vilar, PhD
Principal Researcher in the Associate Laboratory LSRE-LCM

Porto, July 2018

Acknowledgements

My sincere gratitude goes to: Dr. Vítor Vilar, for the work opportunity provided in the LSRE-LCM, for his support and for encouraging me to always try something more in my work; and Dr. Francisca Moreira, for all the guidance, support and tremendous help and patience provided throughout all my time in the laboratory (and outside of it too). Without your assistance and knowledge, the objectives could not have been achieved.

I am also grateful to my colleagues from LSRE (Laboratory E404a and ETAR) for all the fun times and guidance, especially to Larissa for always being so helpful. In special, a big thank you to Sara Santos, my friend and work partner, for all the support, friendship and team work.

My gratitude goes also to my dear Ricardo, for all the inexhaustible patience and tolerance, and unconditional support and love, and to my close friends.

Finally, I would like to express my genuine acknowledgement to my parents, stepparents and my grandmother, without who this would never be possible.

This work was financially supported by: (i) Project POCI-01-0145-FEDER-006984 – Associate Laboratory LSRE-LCM funded by the European Regional Development Fund (ERDF) through COMPETE2020 - Programa Operacional Competitividade e Internacionalização (POCI) – and by national funds through FCT - Fundação para a Ciência e a Tecnologia; and (ii) Project AIProcMat@N2020 - Advanced Industrial Processes and Materials for a Sustainable Northern Region of Portugal 2020, with the reference NORTE-01-0145-FEDER-000006, supported by Norte Portugal Regional Operational Programme (NORTE 2020), under the Portugal 2020 Partnership Agreement, through the ERDF.

Thank you so much!

Abstract

The presence of bromate (BrO_3^-) in drinking waters is a major global concern for human health that requires an effective solution. Photocatalysis is being addressed as a particular interesting process for the reduction of inorganic compounds, including BrO_3^-, due to its improved performance.

The current dissertation focuses on the application of heterogeneous photocatalysis for BrO_3^- reduction in aqueous solution using a commercial Kenics® static mixer (SM) made of stainless steel as support for TiO_2-P25 photocatalyst. The Kenics® SM was assembled in a tubular photoreactor under simulated sunlight coupled to a compound parabolic collector (CPC). This photocatalytic system reduced mass and photon transfer limitations by enhancing pollutants/reactants diffusion and illumination efficiency, respectively. Synthetic aqueous solutions containing 200 µg L^{-1} (1.56 µM) of BrO_3^- in ultrapure water were employed. BrO_3^- photocatalytic reduction was evaluated in terms of BrO_3^- concentration decay and bromide (Br^-) concentration rise.

The TiO_2-P25 films, which were deposited by dip-coating technique, showed a high adherence and stability, allowing results replication over a high number of usages. Total or almost total BrO_3^- reduction into Br^- was always attained.

The effect of the following operational parameters on the efficiency of BrO_3^- photocatalytic reduction was assessed: (i) SM treatment before TiO_2-P25 coating, (ii) number of TiO_2-P25 layers deposited by dip-coating, (iii) position of the SM during the coating procedure, (iv) pH, (v) dissolved oxygen (DO) content at various pH, and (vi) addition of formic acid (HCOOH) as organic sacrificial agent. BrO_3^- removal was improved by applying a thermal pre-treatment to the SM compared to the use of a thermal + chemical pre-treatment, suggesting the formation of better photocatalytic films. Faster BrO_3^- reductions were achieved for increasing number of TiO_2-P25 layers up to 6 layers, for which occurred the maximum absorption of photons by the catalyst. Using the SM in the vertical position during the dip-coating procedure was beneficial compared to its use in the horizontal position, likely due to the formation of a ticker layer near the edges of the SM. The process efficiency was increased for decreasing pH values from 7.0 to 4.0. This can be mainly attributed to the positive charge of the TiO_2 surface at pH below the point of zero charge (PZC) of TiO_2-P25, i.e. 6.2-6.4, thereby attracting BrO_3^-. The presence of high DO levels (212-239 µM, corresponding to experiments in the absence of N_2 supply) was prejudicial for pH 6.5 and 7.0 compared to the presence of null/almost null levels of DO (<3.1 µM, corresponding to experiments in the presence of N_2 supply). For pH 3.0, 4.0 and 5.5, the effect of DO was negligible. This can be related to a stronger adsorption of BrO_3^- onto the TiO_2-P25 surface at pH below 6.2-6.4 (PZC of TiO_2-P25), with BrO_3^- taking advantage in the competition with the DO for electrons (e^-). The use of HCOOH as organic sacrificial agent at pH 6.5 did not improve BrO_3^- removal either in the presence or absence of high levels of DO, suggesting that the weak adsorption of BrO_3^- onto TiO_2 surface that occur at pH 6.5 did not allow to take advantage of the carbon dioxide radical anion ($CO_2^{-\bullet}$) formation, higher amounts of e^- and lower susceptibility of Br^- reoxidation to BrO_3^- that occur in the presence of HCOOH.

Keywords: Heterogeneous photocatalysis; Catalyst support; Titanium dioxide; Static mixer; Bromate reduction.

Resumo

A presença de bromatos (BrO_3^-) em águas potáveis gera uma grande preocupação para a saúde humana a nível mundial que requer uma solução eficaz. Devido à sua eficiência comprovada, a fotocatálise tem ganho particular interesse na redução de compostos inorgânicos, incluindo BrO_3^-.

A presente dissertação foca-se na aplicação da fotocatálise heterogénea para a redução de BrO_3^- em soluções aquosas, usando um misturador estático (ME) comercial Kenics® de aço inoxidável como suporte para o fotocatalisador TiO_2-P25. O ME Kenics® foi colocado no interior de um fotoreator tubular acoplado a um coletor parabólico composto sob luz solar simulada. O sistema fotocatalítico permitiu a redução das limitações da transferência de massa e fotões devido à melhoria da difusão de poluentes/reagentes e eficiência na iluminação, respetivamente. Foram aplicadas soluções aquosas sintéticas contendo 200 µg L^{-1} (1,56 µM) de BrO_3^- em água ultrapura. A redução fotocatalítica de BrO_3^- foi avaliada em termos da diminuição da concentração de BrO_3^- e aumento da concentração de brometos (Br^-).

Os filmes de TiO_2-P25, depositados pela técnica de *dip-coating*, apresentaram elevada aderência e estabilidade, permitindo a reprodução de resultados ao longo de um grande número de usos. Verificou-se sempre a redução total ou quase total de BrO_3^- a Br^-.

Foi avaliado o efeito das seguintes condições experimentais na eficiência da redução fotocatalítica de BrO_3^-: (i) tratamento do ME antes da deposição de TiO_2-P25, (ii) número de camadas de TiO_2-P25 depositadas por *dip-coating*, (iii) posição do ME durante o procedimento de deposição, (iv) pH, (v) oxigénio dissolvido (OD) a vários pH, e (v) adição de ácido fórmico (HCOOH) como agente orgânico sacrificante. A remoção de BrO_3^- melhorou com a aplicação de um pré-tratamento térmico ao ME quando comparado com um pré-tratamento térmico + químico, sugerindo a formação de um melhor filme fotocatalítico. Obtiveram-se reduções mais rápidas de BrO_3^- para um maior número de camadas de TiO_2-P25 até 6 camadas, para as quais ocorreu máxima absorção de fotões pelo catalisador. A utilização do ME na posição vertical durante a deposição foi benéfica em comparação ao seu uso na horizontal, provavelmente devido à formação de uma camada mais espessa nos bordos do ME. A eficiência aumentou com o decréscimo do pH de 7,0 para 4,0. Isto pode dever-se à carga positiva da superfície do TiO_2 a valores de pH abaixo do ponto de carga zero (PCZ) do TiO_2-P25, i.e. 6,2-6,4, atraindo mais BrO_3^-. A presença de níveis elevados de OD (212-239 µM, correspondendo a ensaios sem fornecimento de N_2) foi prejudicial para pH 6,5 e 7,0 quando comparada com a presença nula/quase nula de OD (<3.1 µM, correspondendo a ensaios com fornecimento de N_2). Para pH 3,0, 4,0 e 5,5, o efeito do OD foi desprezável. Isto pode estar relacionado com a maior adsorção dos BrO_3^- à superfície do TiO_2-P25 para valores de pH abaixo de 6,2-6,4 (PCZ do TiO_2-P25), com os BrO_3^- a ganhar vantagem na competição com o OD pelos eletrões (e^-). O uso de HCOOH como agente orgânico sacrificante a pH 6,5 não melhorou a remoção de BrO_3^- na presença ou ausência de níveis elevados de OD, sugerindo que a fraca adsorção dos BrO_3^- à superfície do catalisador para pH 6,5 não permitiu que se tirasse partido da formação do radical anião do dióxido de carbono ($CO_2^{-\bullet}$), das maiores quantidades de e^- e da menor suscetibilidade para a reoxidação de Br^- a BrO_3^- que ocorre na presença de HCOOH.

Palavras-chave: Fotocatálise heterogénea; Suporte para catalisador; Dióxido de titânio, Misturador estático; Redução de bromatos.

Table of Contents

1. Introduction 1
1.1. Bromate ion 1
1.1.1. Approaches to reduce bromate ion levels in waters 2
1.2. Photocatalysis 3
1.2.1. Photocatalysts 5
1.2.1.1. Titanium dioxide 5
1.2.1.2. Photocatalysis limitations 5
1.2.1.3. Influence of operational parameters on photocatalysis 6
1.2.1.3.1. Light intensity and wavelength 6
1.2.1.3.2. Photocatalysts and pollutants loading 6
1.2.1.3.3. Temperature 7
1.2.1.3.4. pH 7
1.2.1.3.5. Dissolved oxygen 7
1.3. Reactors and supports for photocatalysis 8
1.3.1. Reactors limitations 8
1.3.1.1. Photon transfer limitations 8
1.3.1.2. Mass transfer limitations 8
1.3.2. Photocatalytic reactors 9
1.3.3. Catalyst thin film supports 9
1.3.3.1. Static mixers 9
1.4. Photocatalysis applied to the reduction of bromate ion 11
1.5. Objectives and outline 14
2. Materials and methods 15
2.1. Chemicals 15
2.2. Photocatalytic films preparation 18
2.3. Photocatalytic system 20
2.3.1. Experimental procedure 21
2.4. Analytical determinations 22
2.5. Determination of pseudo-first-order kinetic constants 23
3. Results and discussion 25
3.1. General considerations 25
3.2. Influence of static mixer pre-treatment 30
3.3. Influence of number of layers deposited on the static mixer by dip-coating 33

3.4. Influence of static mixer position during dip-coating 36
3.5. Influence of pH 38
3.6. Influence of dissolved oxygen content 40
3.7. Influence of the addition of an organic sacrificial agent – Formic acid 42
4. Conclusions 47
5. Suggestions for future work 49
6. References 51
Appendix 57
Appendix A.I – Calculations for static mixer 59

List of Figures

Figure 1.1 – Mechanisms of BrO_3^- formation during ozonation. Black lines show the direct pathway. Adapted from Pinkernell et al. [5], Copyright © (2001), with permission from American Chemical Society. 1

Figure 1.2 – Scheme of the photocatalytic process at the PCT surface..... 4

Figure 1.3 – Annual number of articles published in the subject areas "Photocatalysis" and "Photocatalysis with TiO_2" in the period 2010-2018. Data collected from Scopus (http://www.scopus.com/), in June 2018..... 5

Figure 2.1 – Kenics® SM as obtained (polished SM) and after sanded treatment (sanded SM). 18

Figure 2.2 – Dip-coating method with Kenics® SM vertically (a) and horizontally (b). 19

Figure 2.3 – Sketch of the laboratorial flow system..... 20

Figure 3.1 – Influence of photolysis on BrO_3^- reduction in the presence (■,□) or absence (●,○) of the SM. Solid symbols: BrO_3^- concentration. Open symbols: Br^- concentration. Conditions: $[BrO_3^-]_0$: 1.56 µM; SM pre-treatment: Thermal (when applicable); pH: 5.5; [DO]: 212-239 µM; Simulated sunlight; *T*: 25 ºC; *Q*: 50 L h^{-1}..... 26

Figure 3.2 – Kenics® SM appearance after thermal pre-treatment and after the application of 3 layers to pre-treated SM with thermal (T) treatment or thermal + chemical (T+C) treatment.... 30

Figure 3.3 – Replicates of TiO_2 PC applied to BrO_3^- reduction using different SM pre-treatments. Solid symbols: BrO_3^- concentration. Open symbols: Br^- concentration. SM pre-treatment: thermal (a), thermal + chemical (b). Replicates: 1st (■,□), 2nd (●,○), 3rd (▲,△). Conditions: $[BrO_3^-]_0$: 1.56 µM; SM position during dip-coating: Vertical; Number of layers: 3; pH: 5.5; [DO]: 212-239 µM; Simulated sunlight; *T*: 25 ºC; *Q*: 50 L h^{-1}. 31

Figure 3.4 – Influence of SM pre-treatment on BrO_3^- reduction by TiO_2 PC. Solid symbols: BrO_3^-concentration. Open symbols: Br^- concentration. SM pre-treatment: thermal (■,□), thermal + chemical (●,○). Conditions: $[BrO_3^-]_0$: 1.56 µM; SM position during dip-coating: Vertical; Number of layers: 3; pH: 5.5; [DO]: 212-239 µM; Simulated sunlight; *T*: 25 ºC; *Q*: 50 L h^{-1}. 1st replicate of each condition was used. 32

Figure 3.5 – Kenics® SM appearance after 1, 3, 6 and 12 layers. 33

Figure 3.6 – Replicates of TiO_2 PC applied to BrO_3^- reduction using SM with different number of layers deposited by dip-coating. Solid symbols: BrO_3^- concentration. Open symbols: Br^- concentration. Number of layers: 1 (a), 6 (b), 12 (c) (replicates of 3 layers are represented in Figure 3.3b). Replicates: 1st (■,□), 2nd (●,○), 3rd (▲,△). Conditions: $[BrO_3^-]_0$: 1.56 µM; SM pre-treatment: Thermal; SM position during dip-coating: Vertical; pH: 5.5; [DO]: 212-239 µM; Simulated sunlight; *T*: 25 ºC; *Q*: 50 L h^{-1}. 33

Figure 3.7 – Influence of number of layers deposited on the SM by dip-coating on BrO_3^- reduction by TiO_2 PC. Solid symbols: BrO_3^- concentration. Open symbols: Br^- concentration. Number of layers: 1 (■,□), 3 (●,○), 6 (▲,△), 12 (◆,◇). Conditions: $[BrO_3^-]_0$: 1.56 µM; SM pre-treatment: Thermal; SM position during dip-coating: Vertical; pH: 5.5; 1st Replicate;

[DO]: 212-239 µM; Simulated sunlight; *T*: 25 ºC; *Q*: 50 L h^{-1}. 1st replicate of each condition was applied. 34

Figure 3.8 – Adsorption of BrO_3^- on the TiO_2 PCT assessed by recirculating the BrO_3^- solution in the dark using the SM coated with different number of layers: 1 (■), 3 (●), 6 (▲), 12 (◆). Conditions: $[BrO_3^-]_0$: 1.56 µM; SM pre-treatment: Thermal; SM position during dip-coating: Vertical; pH: 5.5; [DO]: 212-239 µM; Simulated sunlight; *T*: 25 ºC; *Q*: 50 L h^{-1} 35

Figure 3.9 – Kenics® SM appearance after 6 layers deposition according to the position: vertical (left), and horizontal (right). 36

Figure 3.10 – Replicates of TiO_2 PC applied to BrO_3^- reduction using SM in horizontal position during dip-coating. Solid symbols: BrO_3^- concentration. Open symbols: Br^- concentration. Replicates: 1st (■,□), 2nd (●,○), 3rd (▲,△). Conditions: $[BrO_3^-]_0$: 1.56 µM; SM pre-treatment: Thermal; Number of layers: 6; pH: 5.5; [DO]: 212-239 µM; Simulated sunlight; *T*: 25 ºC; *Q*: 50 L h^{-1} 36

Figure 3.11 – Influence of SM position during dip-coating on BrO_3^- reduction by TiO_2 PC. Solid symbols: BrO_3^- concentration. Open symbols: Br^- concentration. SM position during dip-coating: vertical (■,□), horizontal (●,○). Conditions: $[BrO_3^-]_0$: 1.56 µM; SM pre-treatment: Thermal; Number of layers: 6; pH: 5.5; [DO]: 212-239 µM; Simulated sunlight; *T*: 25 ºC; *Q*: 50 L h^{-1}. 1st replicate of each condition was applied. 37

Figure 3.12 – Influence of pH on BrO_3^- reduction by TiO_2 PC. Solid symbols: BrO_3^- concentration. Open symbols: Br^- concentration. pH: 3.0 (■,□), 4.0 (●,○), 5.5 (▲,△), 6.5 (◆,◇), 7.0 (★,☆). Conditions: $[BrO_3^-]_0$: 1.56 µM; SM pre-treatment: Thermal; SM position during dip-coating: Vertical; Number of layers: 6; [DO]: 212-239 µM; Simulated sunlight; *T*: 25 ºC; *Q*: 50 L h^{-1}. 1st replicate of each condition was applied. 38

Figure 3.13 – Effect of pH on energy of TiO_2 in terms of vacuum level and normal hydrogen electrode level in electrolyte. Adapted from Bak et al. [78], Copyright © (2002), with permission from Elsevier. 39

Figure 3.14 – Influence of DO content on BrO_3^- reduction by TiO_2 at various pH values: 3.0 (a), 4.0 (b), 5.5 (c), 6.5 (d), 7.0 (e). Solid symbols: BrO_3^- concentration. Open symbols: Br^- concentration. [DO]: 212-239 µM (absence of N_2) (■,□), <3.1 µM (presence of N_2) (●,○). Conditions: $[BrO_3^-]_0$: 1.56 µM; SM pre-treatment: Thermal; SM position during dip-coating: Vertical; Number of layers: 6; Simulated sunlight; *T*: 25 ºC; *Q*: 50 L h^{-1}. 1st replicate of each condition was applied. 41

Figure 3.15 – DO content for TiO_2 photocatalytic experiments of Figure 3.14 in the absence of N_2. pH: 3.0 (■), 4.0 (●), 5.5 (▲), 6.5 (◆), 7.0 (★). 41

Figure 3.16 – Influence of addition of different contents of HCOOH at pH 6.5 for [DO] <3.1 µM (presence of N_2) on BrO_3^- reduction by TiO_2 PC in terms of BrO_3^- concentration (solid symbols) and Br^- concentration (open symbols) (a), and $HCOOH^a$ concentration (b). HCOOH:BrO_3^- molar ratio: absence of HCOOH addition (●,○), 3:1 (▲,△), 1:1 (◆,◇), 0.5:1 (★,☆). Conditions: $[BrO_3^-]_0$: 1.56 µM; SM pre-treatment: Thermal; SM position during dip-coating: Vertical; Number of layers: 6; Simulated sunlight; *T*: 25 ºC; *Q*: 50 L h^{-1}. 1st replicate of each condition was applied. 43

Figure 3.17 – Influence of the addition of different contents of HCOOH at pH 6.5 for [DO] of 212-239 µM (absence of N_2) on BrO_3^- reduction by TiO_2 PC in terms of BrO_3^- concentration (solid symbols) and Br^- concentration (open symbols) (a), and HCOOH[a] concentration (b). HCOOH:BrO_3^- molar ratio: absence of HCOOH addition (●,○), 3:1 (▲,△), 0.5:1 (★,☆). Conditions: $[BrO_3^-]_0$: 1.56 µM; SM pre-treatment: Thermal; SM position during dip-coating: Vertical; Number of layers: 6; Simulated sunlight; *T*: 25 ºC; *Q*: 50 L h^{-1}. 1st replicate of each condition was applied. 44

Figure A.1 – Scheme of the SM with its dimensions. 59

List of Tables

Table 1.1 - Bromine oxidation states. 1

Table 1.2 - Studies on the remediation of waters contaminated with BrO_3^- by PC. 12

Table 2.1 - Physicochemical properties of sodium bromate. 15

Table 2.2 - Main physicochemical characteristics of the ultrapure water spiked with BrO_3^-. ... 16

Table 2.3 - Physicochemical properties of various chemicals. 17

Table 2.4 - Dimensions of photoreactor elements. 21

Table 2.5 - Analytical determinations. 22

Table 2.5.1 - Analytical parameters of BrO_3^-, Br^- and $HCOO^-$ calibration curves. 22

Table 3.1 - Pseudo-first-order kinetic constants for bromate concentration decay ($k_{bromate}$) calculated for reductions present in this thesis along with the corresponding time interval of adjustment, residual variance (S^2_R) and coefficient of determination (R^2). 27

Table 3.2 - BrO_3^- redox potentials according to pH. 39

Notation

Acronyms

$[Br^-]_0$	Initial bromide concentration (μM)
$[BrO_3^-]_0$	Initial bromate concentration (μM)
[DO]	Dissolved oxygen concentration (μM)
ARPs	Advanced reduction processes
BPC	By-product compound
CB	Conduction band
CPC	Compound parabolic collector
DO	Dissolved oxygen
HPC	Heterogeneous photocatalysis
LEDs	Light-emitting diodes
M	Inorganic compound
PC	Photocatalysis
PCT	Photocatalyst
PTFE	Polytetrafluoroethylene
PZC	Point of zero charge
$R^\bullet$	Strong reducing species formed from the sacrificial agents
ROS	Reactive oxidizing species
SA	Sacrificial agent
SM	Static mixer
UV	Ultraviolet
VB	Valence band

Symbols

e^-	Electron of conduction band
h^+	Hole of valence band
$k_{bromate}$	Pseudo-first-order kinetic constants for bromate concentration decay (min^{-1})
Q	Flow rate ($L\ h^{-1}$)
R^2	Coefficient of determination (dimensionless)
S^2_R	Residual variance (μM^2)
T	Temperature (ºC)
t	Time (min)

Chemical names

Br	Bromine
Br^-	Bromide
$Br^\bullet$	Bromine radical
BrO^-	Hypobromite
$BrO^\bullet$	Bromine oxide radical
BrO_2^-	Bromite
BrO_3^-	Bromate
CdS	Cadmium sulfide
CO_2	Carbon dioxide
$CO_2^{\bullet-}$	Carbon dioxide radical anion
Fe_2O_3	Ferric oxide
H_2	Hydrogen

H_2O	Water
H_2O_2	Hydrogen peroxide
H_2SO_4	Sulfuric acid
$HCOO^-$	Formate
HCOOH	Formic acid
HO^-	Hydroxide ion
$HO^\bullet$	Hydroxyl radical
HOBr	Hypobromous acid
$HOO^\bullet$	Hydroperoxyl radical
$KBrO_3$	Potassium bromate
N_2	Nitrogen
$NaBrO_3$	Sodium bromate
O_2	Oxygen
$O_2^{\bullet-}$	Superoxide radical
O_3	Ozone
TiO_2	Titanium dioxide
ZnO	Zinc oxide
ZnS	Zinc sulfide

1. INTRODUCTION

1.1. Bromate ion

Bromate ion (BrO_3^-) is a by-product compound (BPC) with a molecular weight of 127.901 g mol^{-1}. It is stable in water, highly soluble at room temperature, non-volatile and it can be slightly adsorbed onto sediment or soil, where it is expected to be mobile [1–4].

BrO_3^- occurs as a result of disinfection processes applied to waters containing bromide (Br^-), such as (i) ozonation (the most common one), (ii) hypochlorination, and (iii) ozonation followed by hypochlorination and/or chloramination [4,5]. It mainly results from drinking water production, although also from industrial and domestic wastewaters treatment and swimming pools sanitation [6]. BrO_3^- formation during ozonation can occur by two mechanisms that may happen separately or in simultaneous, illustrated in Figure 1.1, and with up to six oxidation states of bromine (Br) (Table 1.1). In the direct mechanism, Br^- is oxidized by ozone (O_3) to hypobromous acid and/or hypobromite ($HOBr/BrO^-$), depending on the solution pH, which is then oxidized to bromite (BrO_2^-) by O_3 at a low rate. The indirect mechanism occurs via free radical pathway, where Br^- is oxidized by the hydroxyl radical ($HO^\bullet$) to its radical ($Br^\bullet$), which then reacts with Br^- or O_3, forming $HOBr/BrO^-$ or bromine oxide radical ($BrO^\bullet$), respectively, with the latest forming BrO_2^- via a disproportionation ($2BrO^\bullet \rightarrow BrO^- + BrO_2^-$). For both pathways, the formed BrO_2^- is rapidly oxidized by O_3 to BrO_3^- [4,5,7–9].

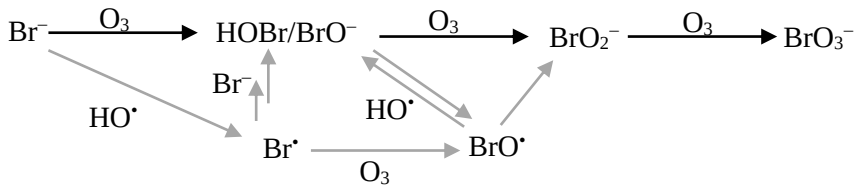

Figure 1.1 - Mechanisms of BrO_3^- formation during ozonation. Black lines show the direct pathway. Adapted from Pinkernell et al. [5], Copyright © (2001), with permission from American Chemical Society.

Table 1.1 - Bromine oxidation states.

Species	Chemical formula
Bromide	Br^-
Hypobromous acid	HOBr
Hypobromite	BrO^-
Bromite	BrO_2^-
Bromine radical	$Br^\bullet$
Bromine oxide radical	$BrO^\bullet$
Bromate	BrO_3^-

Br is part of the common halogen elements, occurring naturally as 50.57% ^{79}Br and 49.43% ^{81}Br [10]. It can be naturally found in waters (seawater, salt lakes, freshwater, groundwater), atmosphere, organic soil and biomass (organisms and plants), mainly as

Br^- [11,12]. Br, and therefore Br^-, levels may increase as a result of: (i) natural processes, such as salt water intrusions (for coastal groundwaters) and local geological situations (for freshwaters) for instance, and (ii) anthropogenic activities, such as potassium and coal mining [6,8]. Furthermore, Br^- has been widely used in aquifers as a tracer [4], and also in swimming pools to produce more persistent disinfectants (bromamine/aqueous bromine, for example) [6].

Br^- levels in the source water determine whether BrO_3^- formation is preoccupant: low levels (< 20 μg L^{-1}) are not problematic; levels between 50 and 100 μg L^{-1} are already of concern; and for levels > 100 μg L^{-1}, the BrO_3^- formation can be a serious problem [8]. In general, higher concentrations of Br^- result in higher concentrations of BrO_3^- [10,11].

Although there is inadequate evidence in humans for the carcinogenicity of potassium bromate, $KBrO_3$, (and, thus, BrO_3^-), there is sufficient evidence in experimental animals [13]. As a result, IARC [13] has evaluated BrO_3^- as possibly carcinogenic to humans even though the mode of the carcinogenetic action has not been discovered yet. Moreover, this DBP is also mutagenic both *in vivo* and *in vitro* [1,13,14]. Hence, its concentration is regulated in drinking water, being the only ozone DBP under legislation [15]. As regulated by the USEPA [16], WHO [1], EU [17] and Portuguese government [18], the maximum BrO_3^- levels in drinking waters are set to 10 μg L^{-1}.

Considering the above-mentioned problems related to BrO_3^-, it is important to study and discover ways to reduce this carcinogenic compound in the environment, especially in drinking waters.

1.1.1. Approaches to reduce bromate ion levels in waters

BrO_3^- minimization and/or removal while maintaining disinfection can be done by: (i) reducing Br^- before BrO_3^- formation, (ii) minimizing BrO_3^- formation during ozonation, and (iii) removing BrO_3^- after ozonation [11,19]. For the first approach, processes such as ion exchange, membrane filtration and precipitation can be applied. On the other hand, the minimization or removal of BrO_3^- (methods (ii) and (iii)) includes: (a) addition of reducing agents, (b) scavenging of $HO^\bullet$, (c) scavenging or reduction of HOBr, which, if present, would lead to BrO_3^- formation according to Figure 1.1, and (d) pH depression [5,7,19,20]. The methods (i) and (ii) only result in a partial minimization of BrO_3^-, while the method (iii) involves BrO_3^- decomposition and it is focused on reduction technologies based on traditional and advanced reduction process (ARPs), such as photolysis, catalysis and photocatalysis [11]. This last approach has been preferable due to the emergent need to reduce BrO_3^- in drinking waters.

1.2. Photocatalysis

Photocatalysis (PC) is a process in which the acceleration of a reaction occurs when a material, a photocatalyst (PCT), interacts with light of sufficient energy (or of a certain wavelength) to produce reactive species that can lead to the photocatalytic transformation of pollutants [21]. The catalyst is a substance that allows the chemical reaction to follow a different path and to proceed faster, while it does not undergo chemical changes and can be recovered in its initial state by the end of the reaction. The major appeal of PC is that it allows the complete mineralization of pollutants to compounds with no environmental harm [22–24].

PC can be (i) homogeneous, where the PCT and the reactant are in the same phase, or (ii) heterogeneous, where they are in different phases. Heterogeneous photocatalysis (HPC) is preferable because it is easier to separate the PCT from the treated solution, which also allows the reuse of the PCT. The photoreaction occurs at the PCT surface [25].

PC has four major mechanisms: photoexcitation, ionization of water, oxygen ionosorption and protonation of superoxide [26]. It is initiated with the illumination of the PCT with photons with energy equal or greater than its band-gap energy ($h\nu \geq E_{bg}$), which leads to the generation of an electron/hole (e^-/h^+) pair. Electrons (e^-) are photoexcited and promoted from the filled valence band (VB) to the empty conduction band (CB), where they are absorbed, creating a positive hole (h^+) in the VB (Eq. 1). The e^-/h^+ pair can migrate to the surface of the PCT and undergo redox reactions with substrates.

For the photocatalytic oxidation of organics, the formation of reactive oxidizing species (ROS) allows the pollutant to be transformed, as it is shown in Eqs. 1-6 and summarized in Figure 1.2. h^+ react with adsorbed water molecule (H_2O) or hydroxide ion (HO^-) to form powerful oxidative $HO^\bullet$, and e^- react with e^- acceptors, such as adsorbed oxygen (O_2) to form superoxide radicals ($O_2^{\bullet-}$). The $HO^\bullet$ react with organic molecules (either adsorbed or close to the surface of the catalyst) without selectivity, causing the mineralization of the organic molecules. The $O_2^{\bullet-}$ take part in the oxidation process, prevent e^-/h^+ recombination, and its protonation produces hydroperoxyl radicals ($HOO^\bullet$) that then transform into hydrogen peroxide (H_2O_2), which dissociates into very reactive $HO^\bullet$. Without H_2O, the photodegradation of organics would not occur because the ROS could not be formed [26,30,32–39,40].

$$\mathrm{PCT} + h\nu \rightarrow h_{VB}^+ + e_{CB}^- \quad (1)$$

$$h_{VB}^+ + (H_2O)_{ads} \rightarrow HO^\bullet_{ads} + H^+_{ads} \quad (2)$$

$$h_{VB}^+ + HO^- \rightarrow HO^\bullet_{ads} \quad (3)$$

$$e^-_{CB} + (O_2)_{ads} \rightarrow O_2^{\bullet-}{}_{ads} \quad (4)$$

$$O_2^{\bullet-}{}_{ads} + H^+ \rightleftharpoons HOO^\bullet_{ads} \quad (5)$$

$$2HOO^\bullet_{ads} \rightarrow (H_2O_2)_{ads} + O_2 \quad (6)$$

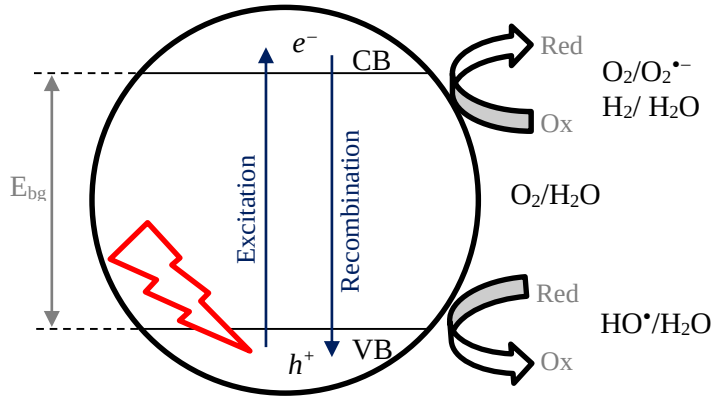

Figure 1.2 - Scheme of the photocatalytic process at the PCT surface.

On the other hand, an inorganic compound M^{n+} can be reduced by e^- to a lower oxidation state if it has a suitable redox potential to make the reaction thermodynamically possible [36]:

$$M^{n+} + e^-_{CB} \rightarrow M^{(n-1)+} \quad (7)$$

Alternatively, M can be oxidized by h^+ or $HO^\bullet$ [36]:

$$M^{n+} + h_{VB}^+ / HO^\bullet_{ads} \rightarrow M^{(n+1)+} \quad (8)$$

Three mechanisms can be considered for the photocatalytic removal of inorganic species according to Dionysiou et al. [36]: (a) direct photoreduction by e^-, (b) indirect photoreduction by intermediates generated by h^+ or $HO^\bullet$ oxidation of e^- donors present in the media, and (c) oxidative removal by h^+ or $HO^\bullet$.

In the direct reduction (a), the initial e^- transfer step, Eq. (7), is usually the rate determining one, with the feasibility of the transformation being governed by the reduction potential of the first step related to the energy of the CB. The h^+ or $HO^\bullet$ can reoxidize also the species to the original one, leading to a non-productive short-circuiting of the overall process:

$$M^{(n-1)} + h_{VB}^+ / HO^\bullet_{ads} \rightarrow M^{n+} \quad (9)$$

The addition of organic sacrificial agents (SAs), commonly carboxylic acids or alcohols, can improve the process since: (i) strong reducing species ($R^\bullet$) can be formed from the SA via Eq. (10), originating an indirect pathway (b), (ii) recombination of e^-/h^+ pairs can be avoided due to the oxidation of the SA by h^+ or $HO^\bullet$ via Eq. (9), increasing the availability of e^- for target species reduction, and (iii) the species reoxidation via Eq. (8) can be also avoided because Eq. (9) is likely to occur.

$$SA + h_{VB}^+ / HO^\bullet_{ads} \rightarrow R^\bullet + H^+ / H_2O \quad (10)$$

In the indirect pathway (b), $R^\bullet$ is the effective reducing species of M^{n+} according to:

$$R^\bullet + M^{n+} \rightarrow R_{ox} + M^{(n-1)+} \quad (11)$$

where R_{ox} can be an aldehyde, a ketone or carbon dioxide (CO_2), depending on the compound. For formic or oxalic acids, the strong reducing carbon dioxide radical anion ($CO_2^{\bullet-}$) is formed. For methanol, ethanol and 2-propanolol, 1-hydroxyalkyl radicals are generated.

The mechanism (c) occurs only for some metals and metalloids and corresponds to the oxidative transformation of M species by h^+ or $HO^\bullet$ according to Eq. (8).

Because PC is a process that uses reactive species in order to destroy and mineralize other compounds, it can be used to a broad variety of areas, such as: (i) oxidation and reduction of

organic and inorganic compounds, (ii) inactivation due to microorganisms' cell wall damaging, (iii) purification and treatment of air and water, (iv) wastewater treatment, (v) active surfaces (self-cleaning materials), (vi) green chemistry (cleaner routes for chemicals production), and (vii) energy conversion (photoreduction of CO_2) [24,25,28].

1.2.1. Photocatalysts

For PC, different PCT can be used (TiO_2, ZnO, Fe_2O_3, CdS and ZnS), being TiO_2 the most researched and used PCT with ca. 49% of the articles about PC being based on it over the last 8 years (see Figure 1.3).

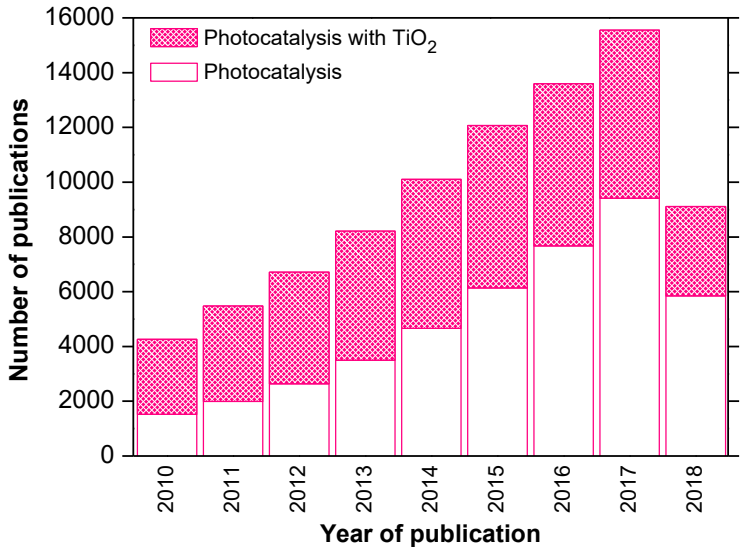

Figure 1.3 - Annual number of articles published in the subject areas "Photocatalysis" and "Photocatalysis with TiO_2" in the period 2010-2018. Data collected from Scopus (http://www.scopus.com/), in June 2018.

1.2.1.1. Titanium dioxide

TiO_2 broad investigation and use occurs because it is applicable in a wide range of technological areas, such as energy, environment and built environment and biomedicine [37], and is the most suitable PCT for environmental applications [30]. This occurs because TiO_2 is cheap, chemically and biologically inert, photoactive, long-term stable against photo- and chemical corrosion, water insoluble, hydrophilic, highly photosensitive, and it is a strong oxidant [19,30,38]. Besides, it is the most active PCT under photon energy between 300 and 390 nm and it remains stable with repeated catalytic cycles [27].

TiO_2 is found in nature as one of the four polymorphs: anatase (tetragonal), brookite (orthorhombic), rutile (tetragonal) and TiO_2 (B) (monoclinic). Rutile is the most stable phase and anatase is the most photoactive [35,39].

1.2.1.2. Photocatalysis limitations

Even though using TiO_2 as a PCT has many advantages, it also has some limitations. A major PC limitation is the recombination of the e^-/h^+ pair, which reduces the efficiency of the process since e^- revert to the VB instead of reacting with adsorbed species, dissipating energy as heat, as shown in Eq. (12) [28,31,32].

$$h_{VB}^+ + e_{CB}^- \rightarrow \text{heat} \qquad (12)$$

While the time for the chemical interaction to occur between TiO_2 and the adsorbed pollutants is in the range of 10^{-8} to 10^{-3} s, the recombination time is on the order of 10^{-9} s, which limits the efficiency of PC [40]. In reductive transformations, e^-/h^+ recombination can be avoided by adding an organic SA, as already discussed in *section 1.2*. Furthermore, O_2 can act as e^- scavenger, as it can be seen in Eq. (4), also hindering recombination.

Another limitation has to do with the fact that it only adsorbs light in the near ultraviolet (UV) (E_{bg} of ca. 3 eV for rutile and ca. 3.2 eV for anatase and brookite), which only represents a small part of the solar spectrum that reaches the Earth's surface (less than 5%) [38,41].

The other limitation has to do with the difficulty in separating the TiO_2 particles from the aqueous phase in heterogeneous PC with the catalysts in suspension. As a result, TiO_2 is being coated on support inert materials [30].

Additionally, PC has a lack of industrial applications as a result of some engineering problems related to (i) the photoreactor design, (ii) scale-up issues, and (iii) the low photocatalytic efficiency when compared to other available technologies [42]. All of these limitations are related with each other.

1.2.1.3. Influence of operational parameters on photocatalysis

1.2.1.3.1. Light intensity and wavelength

Light intensity affects the progress of the photocatalytic reaction and the extent of e^-/h^+ pairs photo-generated and, as a result, the reduction rates because of e^- excitation. Hence, adequate determination of light intensity is crucial to minimize energy consumption and achieve high photocatalytic reaction rates [42–44]. This limitation is linked to the photon transfer one, which is associated with the reactor design, and it is further discussed.

Light wavelength influences the photocatalytic process because the activation of the PCT is dependent on this, which, as a consequence, influences the reaction rate of the process [27].

Light intensity and wavelength are dependent on the light source, being fluorescent UV and mercury arc lamps the most commonly used [45]. Better light sources have been investigated over the years and the use of light-emitting diodes (LEDs) and solar light have gained increasing interest over the researchers [45–47].

1.2.1.3.2. Photocatalysts and pollutants loading

For homogeneous PC, when the amount of the PCT is too high, light cannot penetrate in the reactor due to turbidity and the absorption of photons is not efficient [22,24,48,49]. This drawback can be overcome by immobilizing the PCT on an adequate support. When using it, the layer thickness created directly affects the photocatalytic activity. The increment on the film thickness is beneficial up to a maximum, above which reaction rate becomes independent of it and can even decrease because of the difficulty of the light to penetrate on the PCT layer [24]. Optimum catalyst loading varies between photocatalytic processes and it is mainly dependent on the geometry and working conditions of the photoreactor [27,28].

The irradiation time necessary to achieve complete pollutants removal varies with its initial concentrations, as according to Chong et al. [27]. Excessive concentrations of the water contaminants saturate de PCT surface and reduce the photonic efficiency, which leads to a deactivation of the PCT.

1.2.1.3.3. Temperature

Temperature influences the photocatalytic activity as a result of its effect in (i) e^-/h^+ recombination (increasing temperature results in thermal agitation, promoting recombination), (ii) desorption of adsorbed reactant species (increasing temperature decreases reagents coverage) [24], and (iii) redox potential of species, according to the Nernst equation. Increasing temperature, increases recombination and desorption, leading to a decrease in PC. When the temperature rises above 80 ºC, the rate-limiting step is the exothermic adsorption of reactants. On the other hand, at very low temperatures (below 0 ºC), the rate limiting step is the desorption of the final product. As a result and according to Malato et al. [49], the optimum temperature is generally between 20-80 ºC.

1.2.1.3.4. pH

pH is a very important parameter to consider because it affects many aspects of the photocatalytic process, such as the charge on the catalyst particles, size of catalyst aggregates, positions of CB and VB, and redox potential of pollutants [27,44]. The point at which interactions between water contaminants and PCT is minimal is the so-called point of zero charge (PZC), point at which no electrostatic force is present. TiO_2 surface is positively charged when $pH<pH_{PZC}$, according to Eq. (13), causing an electrostatic attraction force to occur towards negatively charged (anionic) compounds. When $pH> pH_{PZC}$, the surface charge of the PCT is negative, according to Eq. (14), and occurs a repulsion between TiO_2 and anionic compounds [27]. For TiO_2, the pH_{PZC} is within the pH range 4.5-7.0, depending on the properties of TiO_2 [24,27]. For example, for TiO_2-P25, the PZC is in the range of 6.2-6.4 [24,50–52].

$$TiOH + H^+ \rightarrow TiOH_2^+ \quad (13)$$

$$TiOH + HO^- \rightarrow TiO^- + H_2O \quad (14)$$

1.2.1.3.5. Dissolved oxygen

Dissolved oxygen (DO) assures that sufficient e^- scavengers are present in order to avoid recombination, resulting in a higher removal efficiency of the pollutants. Also, it leads to the formation of ROS and the stabilization of radical intermediates. According to Eqs. (5) and (6), the presence of O_2 leads to the formation of $O_2^{\bullet-}$, further protonated to $HOO^\bullet$, which was also reported to have scavenging properties. Hence, DO contributes doubly to avoid recombination in PC, largely influencing the photocatalytic process [27,43].

On the other hand, many authors have reported that for photoreduction, O_2 (and, therefore, DO) is usually not desired because it competes for the photogenerated e^- with the substrate [51,53,54].

DO source usually is the agitation provided to the system [30].

1.3. Reactors and supports for photocatalysis

Consider the design of the photocatalytic reactor, or photoreactor, is important for PC in order to enhance the photocatalytic performance. Reactors have associated limitations that need to be balanced, such as effective photon delivery and mass transfer effects.

1.3.1. Reactors limitations

1.3.1.1. Photon transfer limitations

Photon transfer limitations are related to the low efficiency of illumination because in order to ensure that PC occurs, it is necessary the activation of the PCT by incident light. Effective photons transmission is mainly dependent on reactors design. Even if a PCT is very active, if photons transmission is not effective, the PCT full potential cannot be reached and photocatalytic efficiency is lowered [42,55]. The light that is emitted by the source (natural or artificial) has to travel through the medium that contains reagents and other species, and through the wall of the photoreactor. Because of this, part of the light that is originally emitted is absorbed by the components mentioned earlier before it reaches the PCT [42]. Furthermore, it is necessary at least one of the reactor walls to be transparent so that the chosen radiation can be transmitted, which imposes several limitations to the construction of the reactor [23]. Also, uniform irradiance of the entire PCT surface is very difficult to achieve and, thus, assure the activation of the catalyst is also complicated since uniformity guarantees that a minimum energy for catalyst activation is present [42]. Uniformity can be achieved with the correct position of the light source so that maximum and symmetrical light transmission and distribution can be ensured [27]. Moreover, effective PCT illumination determines the quantity of fluid/gas that will be treated per effective unit area of the PCT [23,56].

Overcoming photon transfer limitations can be achieved using microscale illumination and a large catalyst surface area per unit of reactor volume [42]. Also, microscale illumination has been investigated by applying UV emitting LED devices [57–59] that are able to improve limitations regarding this matter because of the small angle of emittance presented [42]. Moreover, when back side illumination is provided, the pollutants/reagents have to diffuse into the TiO_2 layer to reach the e^-/h^+ pairs, lowering the photocatalytic activity, especially for thick films. Overcoming this can be achieved with front side illumination, in which e^-/h^+ pairs are generated near the liquid-catalyst interface, where the pollutants/reagents are present, reducing the undesirable recombination [42]. As a result, front side illumination is another possible way to overcome photon transfer limitations.

1.3.1.2. Mass transfer limitations

Mass transfer limitations are linked with the limited contact between the e^-/h^+ pairs and the reagents/pollutants, which is influenced by the mixing inside the photoreactor. After the activation of the PCT, the contact between it and the reagents/pollutants needs to be maximized in order to also maximize the removal of the formed reaction products. This issue is mainly related with external (diffusion of the reactants/pollutants from the liquid bulk through a boundary layer to reach the interface between the liquid and the catalyst) and internal (reactants/pollutants inter-particle diffusion within the catalyst film to the active surface sites) mass transfer resistances. Process intensification through the use of novel photoreactors have been proposed to overcome this limitation, such as spinning disc reactors, monolithic photoreactors and microreactors [42]. Improving solution agitation within the reactor, increasing the PCT surface area per unit of rector

volume and reducing diffusional distance between the bulk and catalyst surface are some ways to overcome these limitations. Static mixers (SMs) are being incorporated in chemical engineering industries, since provide effective mixing, increase mass transfer rates and, as a result, minimize mass transfer limitations [60–62].

1.3.2. Photocatalytic reactors

A big number of photocatalytic reactors have been patented and developed over the years. They can generally be divided into three main groups, based on their design characteristics [23,27,63]:

- Distribution of the PCT: (i) slurry systems (with suspended PCT particles), and (ii) immobilized systems (immobilized PCT);
- Type of illumination: artificial or natural (sunlight);
- Position of the light source: (i) immersion-type (placed within the reactor), (ii) external-type (placed outside the reactor), and (iii) distributive-type (light source distributed by optical means to the reactor).

Until recently, slurry systems were preferred because of the high total catalyst surface area per unit of reactor volume. However, the need for a separation unit for the recovery of the PCT and light attenuation through the catalyst suspension are the main disadvantages. Efforts have been made in order to switch to immobilized systems, avoiding the need of a catalyst separation unit although having mass transfer limitations [27,64].

1.3.3. Catalyst thin film supports

The support for catalyst deposition must be carefully selected and certain requirements should be present, such as (i) strong physicochemical interaction with the active phase with no influence in the PCT chemical properties, (ii) high surface area and good sorption capacity for pollutants, (iii) ease of handle and recovery, and (iv) proper geometry to minimize photon and mass transfer limitations. Different supports to immobilize PCT have been used, such as fibbers, membranes, clays, stainless steel and organic polymers, and a multitude of shapes can be applied, such as plates, rings, spheres, monolithic structures and foams [24]. In order to improve the limitations referred, Díez et al [62] have studied the application of a stainless steel SM as a catalyst support for the degradation of the antibiotic oxytetracycline, which provided intense mixing and illumination efficiency, enhancing photon and mass transfer limitations.

1.3.3.1. Static mixers

SMs are motionless devices installed inside reactors that produce consistent and reliable radial mixing by using the energy of the flow to redistribute and divide streamlines. This allows overcoming mass transfer limitations by promoting external and internal mass transfer. Besides, SMs can provide homogeneous feed streams with short residence times. They improve not only mass but also heat transfer operations and work with either laminar or turbulent flows. Other advantages related with this type of mixers are: (i) lower energy consumption, (ii) reduced maintenance because they have no moving parts, (iii) ability to be manufactured from most materials available for construction, and (iv) requirement of smaller space, lower equipment cost and no power except pumping. They are used in continuous processes instead of conventional agitation because analogous and occasionally better performances are obtained with lower costs. The commercially available SMs can be divided into five groups: (i) open designs with helices, (ii) open designs with blades, (iii) corrugated-plates, (iv) multi-layers designs, and (v) closed

designs with channels or holes. The Kenics® SM falls in the first group and was the first ever produced SM, with leader design and technology compared to the remaining ones. It is composed of helically twisted mixing elements placed tightly one after the other so that the top edge of the next insert is perpendicular with the bottom edge of the previous one. This allows the direction of the fluid flow radially towards the pipe walls and to the center, while it simultaneously produces patterns of flow division that grow exponentially for each succeeding element. Intense mixing is provided under both laminar and turbulent flow conditions [60–62,65].

The application of Kenics® SMs under laminar flow conditions is cost saving because the energy required for pumping is reduced. Furthermore, the use of laminar flow regime in HPC can be very advantageous since it can prevent catalyst detachment from the support [62,65,66], and it can help the surface-adsorbed/bound radicals to move into the bulk and form free radicals, which intensifies HPC [61].

1.4. Photocatalysis applied to the reduction of bromate ion

BrO_3^- reduction occurs according to the following equation (E^o = 1.423 V *vs.* SHE) [67]:

$$BrO_3^- + 6H^+ + 6e^- \rightarrow Br^- + 3H_2O \quad (15)$$

A review on a variety of studies regarding the remediation of waters contaminated with BrO_3^- by PC is presented. It comprises features like reactor design and configuration, PCT preparation, and operational parameters such as temperature, pH and light sources. A summary is presented in Table 1.2.

The majority of the cited studies applied commercially available TiO_2 powder, such as Ishihara ST-21 [68,69] and Degussa P25 [19,51,52,70,71] for the photocatalytic reduction of BrO_3^-. On the other hand, Hong et al. [20] synthetized TiO_2 particles from titanium isopropoxide by the sol-gel method. Mills et al. [19] used both PCT powder dispersion and thin films, although the results were not adequately compared.

The photocatalytic efficiency was assessed by examining the reduction of BrO_3^- to Br^- in water, although Parrino et al. [51,70] considered the formation of BrO_3^- in the presence of Br^- (the opposite reaction) and Zhang et al. [52] studied both reactions. These three last studies concluded that Br^- does not react or participate in redox reactions under the operational conditions used. As a result, waters containing Br^- do not generate BrO_3^-. Also, Parrino et al. [70] determined that when waters are contaminated with BrO_3^-, PC is capable to transform it into innocuous Br^- and, if the pH is not too high, organic compounds (such as formic acid, HCOOH) favor the reduction reaction because they act as organic SA.

All of the studies of Table 1.2 concluded that BrO_3^- reduction rate on TiO_2 PCT was highly sensitive to pH. More acidic pH values favor the adsorption of BrO_3^- on the TiO_2 surface, enhancing the BrO_3^- reduction rate. Zhang et al. [52] concluded that the reaction totally stopped at pH 1.5 and 13.5 and that the optimal pH was about 5.5. Likewise, Parrino et al. [51] observed that BrO_3^- reduction did not take place at pH 9.0 in the presence of O_2 (considering a PZC of 6.2). This was mainly explained by the change of the surface charge of the PCT with pH (Eqs. 13 and 14). At pH values higher than PZC, the electrostatic interactions between BrO_3^- and TiO_2 are weak, BrO_3^- adsorption is low and O_2 reduction takes place instead of BrO_3^- reduction.

Three studies proposed modifications on the PCT for BrO_3^- removal. Noguchi et al. [68,69] modified TiO_2 surface with (i) aluminium hydroxide creating alumina-loaded TiO_2 PCT, and (ii) hydrous alumina (pseudo-boehmite), respectively. Mills et al. [19] and Huang et al. [71] used semiconductor PCTs, such as (i) platinised TiO_2 (Pt/TiO_2), and (ii) graphene composites (P25-GR), respectively. BrO_3^- reduction rate was increased with all these techniques when compared with TiO_2 only. Materials loaded on the surface of TiO_2 can act as adsorption centers, increasing the amount of BrO_3^- that is adsorbed on the surface of the modified PCT.

As major conclusion, BrO_3^- photocatalytic reduction can be promoted by two means: (i) controlling water pH or (ii) controlling the surface charge of the PCT without pH control, which can be achieved by loading different materials in the PCT surface.

Table 1.2 - Studies on the remediation of waters contaminated with BrO_3^- by PC.

PCTs & Dose	Light		$[BrO_3^-]_0$; $[Br^-]_0$	Photoreactor	Operational parameters	Ref.
	Position	Type				
ST-21 TiO_2: 0.2 mg TiO_2 per mL potassium nitrate or sulfate Alumina loaded TiO_2: 2.5-40 wt%	n.s.	Artificial: black light fluorescent lamps	$[BrO_3^-]_0$: 0.2 mg L^{-1}	Glass vessel	pH: 5.0-7.0 T: Amb. Irradiation intensity: 0.5 mW cm^{-2}	[68]
ST-21 TiO_2: 0.2 mg TiO_2 in 0.1mM potassium nitrate Pseudo-boehmite loaded TiO_2: 0-1.0 mmol g^{-1} TiO_2	n.s.	Artificial: 10 W black light fluorescent lamps	$[BrO_3^-]_0$: 0.2 mg L^{-1}	Glass vessel	pH: 5.0-7.0 T: Amb. Irradiation intensity: 0.5 mW cm^{-2}	[69]
Platinised TiO_2 [a] in chloroplatinic acid, water and ethanol	TiO_2: 0.5 g chloroplatinic acid: 5 mg ethanol/water (80/20 v/v): 10 cm^3 TiO_2: 0.02 g cm^{-3}	Immersed	Artificial: twelve 8 W 254 nm germicidal lamps	$[BrO_3^-]_0$: 0.05 mg L^{-1}	Cylindrical batch reactor (formed by two half cylinders)	pH: 6.5; 7.8; 7.9; 8.1 T: 20 ºC Irradiation intensity: 14.9 mW cm^{-2} [b]	[19]
	chloroplatinic acid: 2.4 mg ethanol: 4 cm^3 water: 46 cm^3		Artificial: 40 W low-pressure Hg lamp	$[BrO_3^-]_0$: 0.075 mg L^{-1}	Commercial UV sterilizer flow reactor (AquaUV model: UV 605)	Reactor outer wall coated with Pt/TiO_2 Flow rate: 500 cm^3 min^{-1} Irradiation intensity: 1.6 mW cm^{-2}	
P25 TiO_2 (75:25 anatase:rutile): 0.5 g L^{-1} (100 mg dispersed in 200 mL of BrO_3^- or Br^-)		Immersed	Artificial: two low-pressure Hg lamps (254 nm and 365 nm)	$[BrO_3^-]_0$: 1.28x10^4 mg L^{-1} $[Br^-]_0$: 1.28x10^4 mg L^{-1}	Glass bottle wrapped by aluminium foil	pH: 1.5-13.5 T: Amb. Irradiation intensity: 1255 mW cm^{-2} [c] 1150 mW cm^{-2} [d] O_2 or N_2-athmosphere	[52]
P25 TiO_2 (80:20 anatase:rutile): 0.2 g L^{-1} (powder dispersed in the solution)		Immersed	Artificial: medium pressure 125 W Hg lamp	$[BrO_3^-]_0$: 6.40x10^4 mg L^{-1} $[Br^-]_0$: (1.28-12.8)x10^4 mg L^{-1}	Annular batch reactor with Pyrex walls	pH: 6-7.5 [e]; 3.4-3.6 [f] T: 26.85 ºC Flow rate: 300 cm^3 min^{-1} N_2 with pure O_2 or with He–O_2 mixture (80%–20%)	[70]

Table 1.2 - Studies on the remediation of waters contaminated with BrO_3^- by PC.

PCTs & Dose	Light		$[BrO_3^-]_0$; $[Br^-]_0$	Photoreactor	Operational parameters	Ref.
	Position					
P25 TiO_2 (80:20 anatase:rutile): 0.2 g L^{-1} (powder dispersed in the solution)	Immersed	Artificial: medium pressure 125 W Hg lamp	$[BrO_3^-]_0$: (3.84-5.12)x10^4 mg L^{-1}	Annular slurry batch reactor with borosilicate glass walls	pH: low (3.0-4.0); 5.7; 6.0; 9.0 T: 26.85 ºC N_2 with pure O_2 or with He–O_2 mixture (80%–20%)	[51]
Prepared TiO_2 particles from titanium isopropoxide (sol-gel method): 0.6 g dm^{-3} (titanium isopropoxide added to ethanol and water)	Immersed	Artificial: 1000 W high-pressure mercury lamp	$[BrO_3^-]_0$: (2-20)x10^4 mg L^{-1}	Biannular batch pyrex glass reactor	pH: 3-10 T: Amb.	[20]
P25 TiO_2 (75:25 anatase:rutile): 60 mg P25-GR: 0.1 g L^{-1} (dispersed in the solution)	Immersed	Artificial: eight removable 24 W low-pressure Hg lamp	$[BrO_3^-]_0$: 10 mg L^{-1}	Cylindrical batch reactor	pH: 5.1; 6.8; 8.0; 9.2 T: Amb Irradiation intensity: 20 mW cm^{-2} [g]	[71]

[a] Degussa P25 (70:30 anatase:rutile);
[b] For the twelve UV lamps;
[c] For 254 nm lamp;
[d] For 365 nm lamp;
[e] When formate ($HCOO^-$) 0.2-2 mM is used;
[f] When HCCOH 0.1-1 mM is used;
[g] For the two lamps in the center of the reactor
Amb. – Ambient;
n.s. – not specified.

1.5. Objectives and outline

The present dissertation focuses on the application of HPC using TiO_2 fixed on a commercial stainless steel Kenics® SM for the BrO_3^- reduction in aqueous solution. The coated Kenics® SM was assembled in a tubular photoreactor under simulated sunlight coupled to a compound parabolic collector (CPC). To the best of our knowledge, this is the first study regarding the use of a SM as catalyst support for the photocatalytic reduction of an inorganic pollutant. Previously, Díez et al. [62] proved that stainless steel Kenics® SMs can be successfully applied as catalyst supports for HPC in tubular photoreactors with CPCs for the oxidation of organic compounds in aqueous solution – the antibiotic oxytetracycline was used as model compound. The Kenics® SM provided intense mixing even under laminar flow, permitting to overcome mass transfer limitations. Furthermore, the use of a CPC to reflect sunlight ensured that the entire PCT surface area was receiving front side illumination, improving photon transfer.

Synthetic aqueous solutions containing 200 µg L^{-1} (1.56 µM) of BrO_3^- in ultrapure water were used as reaction medium and TiO_2-P25 was used as PCT. The photocatalytic efficiency was assessed by measuring the BrO_3^- and Br^- contents by ion chromatography during reactions. The influence of the following operational parameters on BrO_3^- reduction was evaluated: (i) SM treatment before TiO_2 deposition (thermal *versus* thermal + chemical), (ii) TiO_2 dosage by varying the number of catalyst layers deposited by dip-coating technique (1,3, 6 or 12 layers), (iii) position of the SM during the dip-coating procedure (vertical *versus* horizontal), (iv) pH (3.0, 4.0, 5.5, 6.5 and 7.0), (v) amount of DO at various pHs values, and (vi) addition of HCOOH as organic SA, with the application of various HCOOH:BrO_3^- molar ratios (0.5:1, 1:1 and 3:1). The reusability of the photocatalytic films was also assessed.

The thesis is structured in 5 chapters:

Chapter 1 corresponds to the present introductory section, in which the problem of BrO_3^- present in drinking waters is addressed. Emphasis is given to PC, for which fundamentals and effects of operational parameters are described, and photoreactors and catalyst supports for HPC, including SMs, are surveyed. Finally, a literature review regarding PC applied to BrO_3^- reduction is given.

Chapter 2 describes all chemicals and analytical determinations used within this dissertation as well as the photocatalytic films preparation procedure, the photocatalytic system and respective experimental procedure, and the model used for the determination of pseudo-first-order kinetic constants.

Chapter 3 comprises experimental results and respective discussion, approaching first some general considerations and then the effect of the operational parameters tested on the photocatalytic reduction of BrO_3^-.

Finally, Chapters 4 and 5 display, respectively, the conclusions of the obtained results and some suggestions for future work.

2. MATERIALS AND METHODS

2.1. Chemicals

Table 2.1 presents a summary of some properties of sodium bromate, used as model compound. Solutions of this compound were prepared daily by pipetting the appropriate volume from a stock-solution and diluting it into ultrapure water. Ultrapure water was obtained from a Millipore®-Q system (18.2 MΩ resistivity at 25 ºC) and its main physicochemical characteristics are showed in Table 2.2. This water was used not only to prepare solutions but also to clean the system and all the laboratorial material.

Table 2.1 - Physicochemical properties of sodium bromate.

	Sodium bromate
Molecular structure	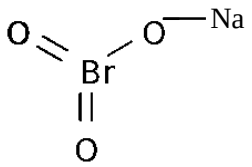
Molecular formula	$NaBrO_3$
Molecular weight (g mol^{-1})	150.90
Purity	>99%
Supplier	Merck

TiO_2 Aeroxide® P25 powder was supplied by Evonik and it was used as delivered. This catalyst exhibited the following characteristics: ≥99.5% (w/w) purity, 80% anatase and 20% rutile crystalline phases, average crystal size of 25 nm, specific surface area of 50 m^2 g^{-1}, and density of 3.9 g cm^{-3}. Other chemicals used throughout this study are briefly described in Table 2.3.

Table 2.2 - Main physicochemical characteristics of the ultrapure water spiked with BrO_3^-.

Parameter (units)	**Ultrapure water**
Color	Colourless
Odor	Odourless
pH	5.8
Conductivity (µS cm^{-1})	0.5
Turbidity (NTU)	0.30
Total dissolved carbon (mg L^{-1})	0.15
Dissolved inorganic carbon (mg L^{-1})	<0.02 [1]
Dissolved organic carbon (mg L^{-1})	0.15
Total dissolved iron (mg L^{-1})	<0.1 [1]
Total suspended solids (mg L^{-1})	n.d.
Total volatile solids (mg L^{-1})	n.d.
Ammonium – N-NH_4^+ (mg L^{-1})	<0.05 [1]
Nitrite – N-NO_2^- (mg L^{-1})	<0.01 [1]
Nitrate – N-NO_3^- (mg L^{-1})	<0.05 [1]
Sulfate – SO_4^{2-} (mg L^{-1})	<0.01 [1]
Chloride – Cl^- (mg L^{-1})	0.16
Phosphate – PO_4^{3-} (mg L^{-1})	<0.2 [1]
Calcium – Ca^{2+} (mg L^{-1})	<0.4 [1]
Magnesium – Mg^{2+} (mg L^{-1})	0.03
Potassium – K^+ (mg L^{-1})	0.07
Sodium – Na^+ (mg L^{-1})	0.32

n.d. – not detected;
[1] Limit of detection value.

Table 2.3 - Physicochemical properties of various chemicals.

Chemical	Molecular formula	Molecular weight (g mol^{-1})	Purity / Concentration	Density (g cm^{-3})	Supplier	Purpose
Surfactant Triton™ X-100	(t-Oct-C_6H_4-$(OCH_2CH_2)_nOH$, n = 9–10	625	-----	1.07	Sigma-Aldrich	Preparation of TiO_2-P25 suspension
Hydrochloric Acid	HCl	36.46	37% (w/w)	1.18	Thermo Fisher Scientific	pH adjustment
Sodium Hydroxide	NaOH	40.00	≥99% (w/w)	1.03	Labkem	pH adjustment
Sulfuric Acid	H_2SO_4	98.07	95% (w/w)	1.83	Fisher Scientific	SM chemical treatment
Bromide standard	Br^-	79.904	(1000±4) mg L^{-1}	0.997–1.001	Sigma-Aldrich	Standard for ion chromatograph
Bromate standard	BrO_3^-	127.901	(1000±4) mg L^{-1}	1.00	Sigma-Aldrich	Standard for ion chromatograph
Formate standard	CHO_2^-	46.03	1000 g L^{-1}	0.999	Fluka	Standard for ion chromatograph
Potassium Hydroxide	KOH	56.11	0.1 N	1.00	Thermo Fisher Scientific	Eluent for ion chromatograph
Nitrogen 5.0	N_2	28.01	≥99.999	-----	The Linde Group	Removal of O_2 from the system
Formic Acid	HCOOH	46.0	99.5%	1.22	VWR Chemicals	Organic SA
Derquim LM 01	-----	-----	-----	-----	Panreac	Alkaline detergent to wash the material

2.2. Photocatalytic films preparation

Kenics® SM (Figure 2.1) was made of plain polished 304 stainless steel, composed of 66-74% of iron, 18-20% of chromium, 8-10% of nickel, among other minor constituents. Previously to catalyst deposition, the SM surface was sanded (Figure 2.1) in order to improve the catalyst adherence. Afterwards, impurities were removed by: (i) cleaning in alkaline detergent solution (alkaline detergent dissolved in ultrapure water), (ii) sonication for 15 min in an ultrasonic cleaning unit Elmasonic S 120 (H) from Elma at 50 kHz, (iii) rinsing with ultrapure water, and (iv) drying at room temperature. Then, the SM was subjected to two different pre-treatments based on Rodriguez et al. [72]: (i) a thermal/heat treatment followed by a chemical treatment, and (ii) a thermal/heat treatment. The thermal/heat treatment was carried out in a furnace using a temperature ramp rate of 2 ºC min^{-1} until it reached 500 ºC and this temperature was maintained for 4 h. Afterwards, the furnace was cooled down up to reach room temperature. The chemical treatment was executed by immersing the SM in a sulfuric acid solution (10 wt. %) for 3 h. In order to eliminate acidic traces, the SM was immersed two times in ultrapure water under sonication for 30 min. Finally, the SM was dried at 100 ºC for 1 h.

A volume of 1 L of TiO_2-P25 aqueous suspension of 2% (w/v) was prepared using ultrapure water and adding 1 drop of Triton™ X-100 per 100 mL of aqueous suspension. This suspension was sonicated for 15 min in an ultrasonic processor VCX 130 from Sonics® at 20 kHz (80% amplitude) to better disperse the particles. TiO_2 deposition was performed by the dip-coating method in an automatic dip-coating unit RDC 15 from Bungard-Elektronik using a speed of insertion and drawing of 50 mm min^{-1} and a layer dipping time of 30 s. The SM was drowned into the TiO_2-P25 suspension either vertically or horizontally, as shown in Figure 2.2. One, three, six or twelve layers were executed. After each layer, the SM was dried at room temperature for ca. 3 min and at 60 ºC for 30 min. Before each experiment and after final number of layers deposited (1, 3, 6 or 12), the SM was placed inside the photoreactor and left recirculating at dark for 3h in ultrapure water, in order to avoid PCT leaching during reactions.

Polished SM **Sanded SM**

Figure 2.1 – Kenics® SM as obtained (polished SM) and after sanded treatment (sanded SM).

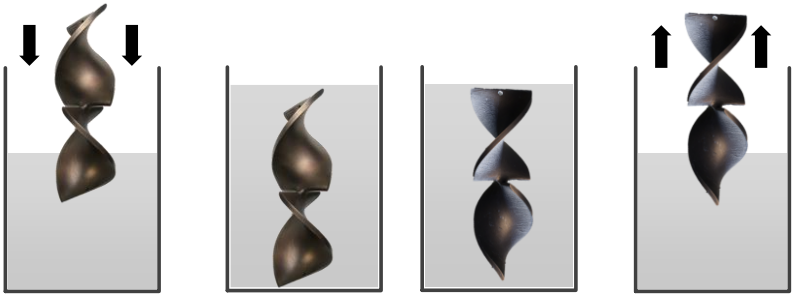

(a)

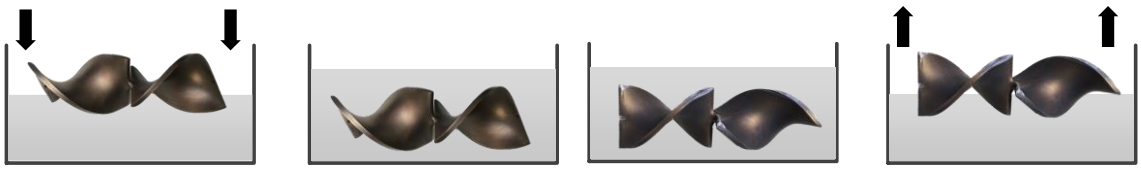

(b)

Figure 2.2 - Dip-coating method with Kenics® SM vertically (a) and horizontally (b).

2.3. Photocatalytic system

Figure 2.3 displays the sketch of the laboratorial flow system. This system was mainly composed of: (i) a jets photoreactor of 0.271 L containing a stainless steel Kenics® SM, (ii) a 1.6 L capacity recirculation cylindrical glass vessel thermostatically controlled and magnetically stirred, (iii) a solar radiation simulator (Suntest XLS + from Atlas) equipped with a 1700 W air-cooled xenon arc lamp at the top, and (iv) a CPC placed below the jets photoreactor. The jets photoreactor consisted in a borosilicate tube (Schott-Durant type 3.3, Germany, cut-off at 280 nm) and two polypropylene caps, each one with two equidistant inlets/outlets. The stainless steel Kenics® SM consisted of two helical mixing elements that provided a total volume of 31 cm^3 and a total surface area of 190 cm^2, delivering a reactor working volume of 0.240 L. Table 2.4 gives some dimensions of the borosilicate tube and the helical mixing elements. From this table, it can be seen that the SM perfectly fitted the borosilicate tube. *Appendix A.I* presents how the dimensions were measured in the SM and some calculations. The sunlight simulator irradiance was set at 500 W m^{-2}, which provided an average radiation intensity at the photoreactor surface of 44 W m^{-2} at wavelengths ranging from 280 to 400 nm. A radiant power of 0.61±0.02 W from 280 to 405 nm was reaching the system, as determined in Díez et al. [62] by 2-nitrobenzaldehyde actinometry using 2.5 mmol L^{-1} of actinometer.

The CPC consisted of two reflectors in the shape of a truncated parabola and showing a surface area of 0.023 m^2. CPC was used to expose all the catalyst surface area to front side illumination, resulting in an illuminated catalyst surface area per unit of reactor volume of 79 m^2 m^{-3}. All the system units were connected by polytetrafluoroethylene (PTFE) tubing. The solution flowed continuously throughout the system by using a gear pump (Ismatec, model BVP-Z).

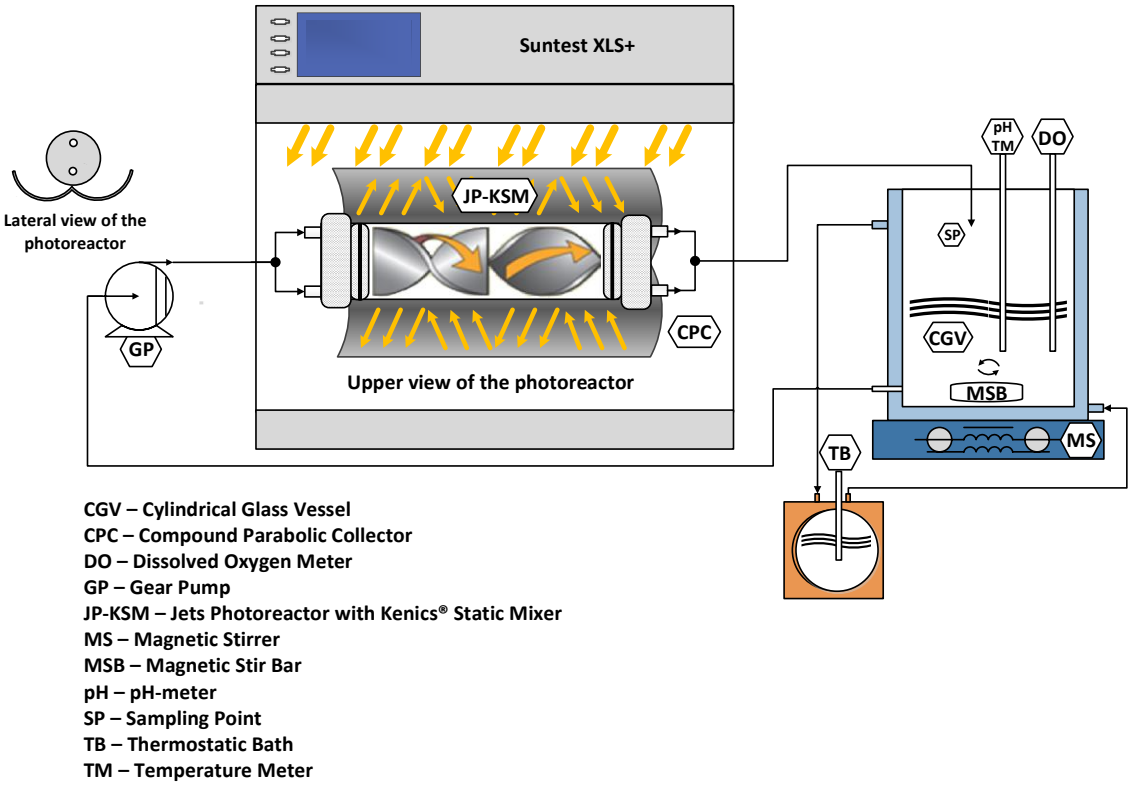

Figure 2.3 - Sketch of the laboratorial flow system.

Table 2.4 - Dimensions of photoreactor elements.

	Borosilicate tube	Helical mixing elements
Internal diameter or Height (cm)	4.64	4.5
Length (cm)	16.0	9.8
Thickness (cm)	0.18	0.35

2.3.1. Experimental procedure

Before starting each reaction, the pH of a prepared BrO_3^- solution of 200 μg L^{-1} (1.56 μM) was adjusted to the pretended one and 1.5 L of this solution were poured into the 1.6 L capacity glass vessel. The thermostatic bath was switched on at a temperature set-point that allowed the solution to reach a temperature of 25.0±0.5 ºC. The system was left un-recirculating until reaching the desired temperature. Afterwards, the gear pump was switched on and the solution was homogenized by recirculation for 10 min in the dark. A 15 mL of control sample was collected, corresponding to time t = 0. The lamp of the solar radiation simulator was switched on at 500 W m^{-2}. 15 mL samples were taken at 15 min, 30 min and then each 30 min until reaching 180 min (3 h). For processes with minimum concentration of DO, N_2 was injected in the glass vessel, which was covered with Parafilm® M before recirculation of the system to allow complete minimization of DO. For experiments with HCOOH addition, a given volume of a HCOOH stock-solution was added to the BrO_3^- solution and the pH of the solution was further adjusted. During reactions, the pH was adjusted to maintain the required value and the temperature of the thermostatic bath was also adjusted to keep the solution at the same temperature. The flow rate was constant for all the experiments and equal to 50 L h^{-1}.

2.4. Analytical determinations

The description of the various analytic determinations used throughout the experimental work are presented in Table 2.5. Additional analyses for ultrapure water characterization were performed according to Moreira et al. [73].

Table 2.5 - Analytical determinations.

Parameter	Methodology
BrO_3^- [a] **Br^- [a]** **$HCOO^-$ [a]**	Ions concentration was followed by ion chromatography by injecting 5 µL samples into a Dionex ICS-2100 liquid chromatograph equipped with (i) a Dionex IonPac AG19 (2×50 mm) + IonPac AS19 (2×250 mm) column at 30 ºC, and (ii) a Dionex Anion Electrolytically Regenerated Suppressor 500 (2 mm) in Auto Suppression Recycle Mode with an applied current of 15 mA. A solution of 20 mM KOH was used as the eluent and the elution was isocratic at a flow rate of 0.30 mL min^{-1} for 8 min. Retention times for formate ($HCOO^-$), BrO_3^- and Br^- were ca. 3.6 min, 4.0 min and 6.2 min, respectively. Calibration curves were determined with 8 concentration levels ranging from 10.0 to 240.0 µg.L^{-1}, in triplicate. The analytical parameters of the working calibration curves are collected in Table 2.5.1. **Table 2.5.1 -** Analytical parameters of BrO_3^-, Br^- and $HCOO^-$ calibration curves.

Ion	Range (µg L^{-1})	Slope ($a \pm s_a$ [a]) (µS L µg^{-1} min^{-1})	Interception ($b \pm s_b$ [b]) (µS min^{-1})	R^2 [c]	s_a/a [d] (%)	LOQ [e] (µg L^{-1})	LOD [f] (µg L^{-1})
BrO_3^-	10.0-240.0	(375±6)×10^{-7}	(-11±9) ×10^{-5}	0.997	1.62	23.0	6.9
Br^-	10.0-240.0	(706±9)×10^{-7}	(-3±1) ×10^{-4}	0.999	1.31	14.5	4.3
$HCOO^-$	10.0-240.0	(100±1)×10^{-6}	(-2±1) ×10^{-4}	0.999	1.09	15.0	4.5

[a] Standard deviation for a ; [b] Standard deviation for b ; [c] Coefficient of determination;
[d] Relative standard deviation of a; [e] Limit of quantification; [f] Limit of detection

Temperature	Temperature was measured by a WTW inoLab 730 laboratory meter.
pH	pH was measured by a WTW inoLab 730 laboratory meter.
DO	DO was determined in a HANNA Instruments HI98194 or HI769928 Multiparameter analyser.

[a] Samples filtration through 0.20 µm Nylon syringe filters from VWR International before analysis.

2.5. Determination of pseudo-first-order kinetic constants

A pseudo-first-order kinetic model was fitted to the experimental data as a simple mathematical model that allows to calculate proper kinetic constants to quantitatively compare the efficiency of BrO_3^- reduction under different photocatalytic processes. This kinetic model was adjusted by a nonlinear regression method using Fig.P software for Windows from Biosoft. The pseudo-first-order kinetic constants for BrO_3^- removal ($k_{bromate}$) in min^{-1} were calculated from Eq. (16):

$$[BrO_3^-]_x = [BrO_3^-]_0 \times e^{-(k_{bromate}) \times x} \quad (16)$$

where $[BrO_3^-]_x$ and $[BrO_3^-]_0$ are BrO_3^- contents after time x and just before reaction start, respectively.

The fitting was performed by minimizing the sum of the squared deviations between experimental and predicted values. The goodness of the fitting was assessed by calculating the relative standard deviations, the coefficient of determination (R^2) and the residual variance (S^2_R).

3. RESULTS AND DISCUSSION

3.1. General considerations

Solutions of 200 μg L^{-1} (1.56 μM) of BrO_3^- in ultrapure water were applied. The main physicochemical properties of the ultrapure water used are presented in Table 2.2.

BrO_3^- reduction was evaluated in terms of BrO_3^- concentration decay and Br^- concentration rise, measured by ion chromatography. In order to better assess the reduction of BrO_3^- to Br^- and the ratios of HCOOH and O_2 to BrO_3^-, the concentrations of these species were considered in μM throughout this dissertation.

Samples treatment before ion chromatography injection was evaluated by different approaches: (i) absence of treatment, and (ii) using 0.20 μm Nylon syringe filters, with the discharge of the first 3 mL of filtered sample. Samples injection in the ion chromatograph was done from sample collected at 180 min to sample collected at 0 min or reversely. All these approaches led to the same result (not shown). The selected treatment procedure was the filtration of samples with 0.20 μm Nylon syringe filters, with the discharge of the first 3 mL of filtered sample, and samples injection in the ion chromatograph from time 180 min to time 0 min.

A flow rate of 50 L h^{-1} (Reynolds number of 380; laminar flow) was used in all trials because it was selected as optimum in Díez et al. [62], where a TiO_2 coated Kenics® SM was used for antibiotic oxytetracycline degradation, providing maximum antibiotic removal, reduced PCT detachment and energy saving costs.

A temperature of 25 ºC was applied since the optimum temperature is in the range 20-80 ºC [49] and the goal was to use ambient temperature.

For trials carried out before the assessment of pH influence on BrO_3^- reductions, the pH was adjusted to 5.5 since Zhang et al. [52] determined this as the optimum pH value for BrO_3^- reduction when using commercial TiO_2-P25 as PCT. Because the PZC for TiO_2-P25 is in the range of 6.2-6.4 [24,50–52], its surface is positively charged at pH 5.5, which means that BrO_3^- adsorption increases, providing higher reduction efficiency. During the experiments, the solution pH suffered some variations and, for this reason, it was regularly adjusted by adding small volumes of 0.02 M NaOH or 0.02 M HCl.

Photolysis was performed both in the absence and presence of the uncoated SM in order to check the capability of BrO_3^- to be reduced only by light and if some anodic dissolution of iron and chromium (the major components of the 304 stainless steel), stimulated by h^+, was occurring, which can affect the process efficiency. Process efficiencies can be reduced because iron and chromium hydroxides, oxides or other inorganic compounds that can be formed on the surface of the PCT under irradiation are synthesized by the e^- that emerge to the surface, diminishing the amount of e^- available to reduce BrO_3^- [74]. Photolysis control experiments (Figure 3.1) revealed very little capacity to reduce BrO_3^- in the absence and presence of the uncoated SM, indicating the inability of BrO_3^- to react with light and the absence of anodic dissolution of iron and chromium that compose the SM. The pseudo-first-order kinetic constants of BrO_3^- concentration decay ($k_{bromate}$) for these control trials can be accessed in Table 3.1, where the $k_{bromate}$ values for all experiments carried out within this dissertation are displayed.

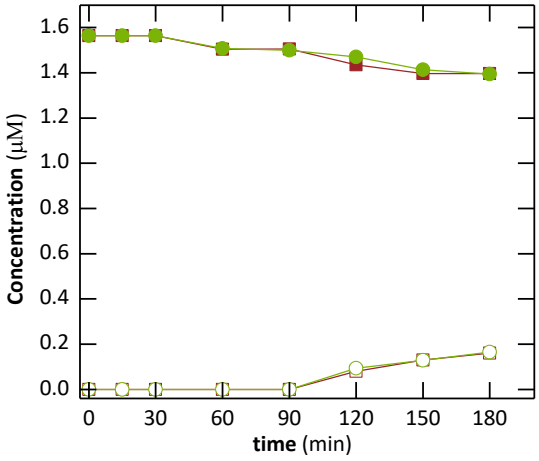

Figure 3.1 – Influence of photolysis on BrO_3^- reduction in the presence (■,□) or absence (●,○) of the SM. Solid symbols: BrO_3^- concentration. Open symbols: Br^- concentration. Conditions: $[BrO_3^-]_0$: 1.56 μM; SM pre-treatment: Thermal (when applicable); pH: 5.5; [DO]: 212-239 μM; Simulated sunlight; *T*: 25 ºC; *Q*: 50 L h^{-1}.

Table 3.1 - Pseudo-first-order kinetic constants for bromate concentration decay ($k_{bromate}$) calculated for reductions present in this thesis along with the corresponding time interval of adjustment, residual variance (S^2_R) and coefficient of determination (R^2).

System			Time interval (min)	$k_{bromate}$ (10^{-3} min^{-1})	S^2_R (μM^2)	R^2
Photolysis [1]		**Presence of SM**	0-15, 60, 150-180	0.65±0.02	0.00029	0.989
		Absence of SM	0-15, 60, 120, 180	0.65±0.03	0.00038	0.983
Influence of SM pre-treatment [2]	**Thermal + chemical pre-treatment**	**1st replicate**	0-180	4.70±0.09	0.0027	0.996
		2nd replicate	0-180	4.86±0.08	0.0019	0.997
		3rd replicate	0-180	4.87±0.05	0.00067	0.999
	Thermal pre-treatment	**1st replicate**	0-180	7.05±0.06	0.00077	0.999
		2nd replicate	0-180	7.3±0.1	0.0032	0.997
		3rd replicate	0-180	7.2±0.1	0.0029	0.998
Influence of number of layers deposited on the SM by dip-coating [3]	**1 layer**	**1st replicate**	0-180	5.13±0.06	0.0011	0.999
		2nd replicate	0-180	5.03±0.08	0.0021	0.998
		3rd replicate	0-180	5..07±0.07	0.0017	0.999
	3 layers	**1st replicate**	0-180	7.05±0.06	0.00077	0.999
		2nd replicate	0-180	7.3±0.1	0.0032	0.997
		3rd replicate	0-180	7.2±0.1	0.0029	0.998
	6 layers	**1st replicate**	0-180	8.84±0.09	0.0011	0.999
		2nd replicate	0-180	8.8±0.1	0.0021	0.999
		3rd replicate	0-180	9.1±0.1	0.0026	0.998
	12 layers	**1st replicate**	0-180	8.5±0.1	0.0025	0.998
		2nd replicate	0-180	8.8±0.1	0.0019	0.999
		3rd replicate	0-180	8.5±0.1	0.0019	0.999

Table 3.1 - Pseudo-first-order kinetic constants for bromate concentration decay ($k_{bromate}$) calculated for reductions present in this thesis along with the corresponding time interval of adjustment, residual variance (S^2_R) and coefficient of determination (R^2).

System			**Time interval** (min)	$k_{bromate}$ (10^{-3} min^{-1})	S^2_R (μM^2)	R^2
Influence of SM position during dip-coating [4]	**Vertical**	**1st replicate**	0-180	8.84±0.09	0.0011	0.999
		2nd replicate	0-180	8.8±0.1	0.0021	0.999
		3rd replicate	0-180	9.1±0.1	0.0026	0.998
	Horizontal	**1st replicate**	0, 60-180	5.4±0.1	0.0035	0.994
		2nd replicate	0, 60-120, 180	5.6±0.1	0.0022	0.996
		3rd replicate	0, 30, 90-180	5.5±0.1	0.0022	0.997
Influence of pH [5, 8]		**pH 3.0**	0-150	17.3±0.8	0.015	0.992
		pH 4.0	0-180	17.1±0.5	0.0062	0.997
		pH 5.5	0-180	8.84±0.09	0.0011	0.999
		pH 6.5	0-30, 90-180	1.97±0.04	0.0011	0.995
		pH 7.0	0-60, 120-180	1.20±0.02	0.00036	0.996
Influence of DO content [6, 8]	**pH 3.0**	**[DO]: 212-239 μM**	0-150	17.3±0.8	0.015	0.992
		[DO]: <3.1 μM	0-150	17.3±0.9	0.019	0.991
	pH 4.0	**[DO]: 212-239 μM**	0-180	17.1±0.5	0.0062	0.997
		[DO]: <3.1 μM	0-180	15.0±0.3	0.0039	0.998
	pH 5.5	**[DO]: 212-239 μM** [8]	0-180	8.84±0.09	0.0011	0.999
		[DO]: <3.1 μM	0-180	8.4±0.1	0.0025	0.998
	pH 6.5	**[DO]: 212-239 μM**	0-30, 90-180	1.97±0.04	0.0011	0.995
		[DO]: <3.1 μM	0-60, 120-180	3.40±0.08	0.0026	0.995
	pH 7.0	**[DO]: 212-239 μM**	0-60, 120-180	1.20±0.02	0.00036	0.996
		[DO]: <3.1 μM	0-90, 150-180	1.64±0.02	0.0035	0.997

Table 3.1 - Pseudo-first-order kinetic constants for bromate concentration decay ($k_{bromate}$) calculated for reductions present in this thesis along with the corresponding time interval of adjustment, residual variance (S^2_R) and coefficient of determination (R^2).

Influence of addition of an organic sacrificial agent – Formic acid [7, 8]	**[DO]: <3.1 µM**	**Absence of HCOOH**	0-60, 120-180	3.40±0.08	0.0026	0.995
		HCOOH:BrO_3^- molar ratio: 3:1	0-180	2.27±0.04	0.0012	0.996
		HCOOH:BrO_3^- molar ratio: 1:1	0-30, 90-180	3.27±0.05	0.0013	0.997
		HCOOH:BrO_3^- molar ratio: 0.5:1	0-180	3.60±0.07	0.0026	0.995
	[DO]: 212-239 µM	**Absence of HCOOH**	0-30, 90-180	1.97±0.04	0.0011	0.995
		HCOOH:BrO_3^- molar ratio: 3:1	0-60, 150-180	1.37±0.03	0.00045	0.996
		HCOOH:BrO_3^- molar ratio: 0.5:1	0-180	2.10±0.05	0.0021	0.991

[1] Conditions: $[BrO_3^-]_0$: 1.56 µM; SM pre-treatment: Thermal (when applicable); pH: 5.5; [DO]: 212-239 µM; Simulated sunlight; *T*: 25 ºC; *Q*: 50 L h^{-1};
[2] Conditions: $[BrO_3^-]_0$: 1.56 µM; SM position during dip-coating: Vertical; Number of layers: 3; pH: 5.5; [DO]: 212-239 µM; Simulated sunlight; *T*: 25 ºC; *Q*: 50 L h^{-1};
[3] Conditions: $[BrO_3^-]_0$: 1.56 µM; SM pre-treatment: Thermal; SM position during dip-coating: Vertical; pH: 5.5; [DO]: 212-239 µM; Simulated sunlight; *T*: 25 ºC; *Q*: 50 L h^{-1};
[4] Conditions: $[BrO_3^-]_0$: 1.56 µM; SM pre-treatment: Thermal; Number of layers: 6; pH: 5.5; [DO]: 212-239 µM; Simulated sunlight; *T*: 25 ºC; *Q*: 50 L h^{-1};
[5] Conditions: $[BrO_3^-]_0$: 1.56 µM; SM pre-treatment: Thermal; SM position during dip-coating: Vertical; Number of layers: 6; [DO]: 212-239 µM; Simulated sunlight; *T*: 25 ºC; *Q*: 50 L h^{-1};
[6] Conditions: $[BrO_3^-]_0$: 1.56 µM; SM pre-treatment: Thermal; SM position during dip-coating: Vertical; Number of layers: 6; Simulated sunlight; *T*: 25 ºC; *Q*: 50 L h^{-1};
[7] Conditions: $[BrO_3^-]_0$: 1.56 µM; SM pre-treatment: Thermal; SM position during dip-coating: Vertical; Number of layers: 6; pH: 6.5; Simulated sunlight; *T*: 25 ºC; *Q*: 50 L h^{-1};
[8] 1st replicate of each condition was applied.

3.2. Influence of static mixer pre-treatment

In order to increase SM surface roughness and help to attach the PCT to the SM surface, preventing PCT detachment, the sanded SM was subjected to treatments before TiO_2 deposition. As a result, two pre-treatment techniques were conducted by following Rodriguez et al. [72] with some little variations, as explained in *section 2.2*: (i) a thermal treatment followed by a chemical treatment, and (ii) a thermal treatment. Rodriguez et al. [72] concluded that increasing the surface roughness of stainless steel plates was more efficient by using thermal treatment followed by chemical treatment than chemical treatment only. This occurred because a smoother surface morphology for the stainless steel was obtained after chemical treatment without previous thermal treatment. Taking these results into account, the application of a chemical treatment was not contemplated in the current study.

The appearance of the SM after the thermal pre-treatment is displayed in Figure 3.2. The aspect of the SM after the thermal + chemical pre-treatment is not presented since we do not have a picture of it. It is worth mentioning that it had a dark-brown color that immediately disappeared after the cleaning treatment (rising with water, as explained in *section 2.2*), looking similar to the SM after thermal pre-treatment. For the comparison of the two pre-treatments, 3 layers were applied to the SM. The appearance of the SM after the deposition of 3 layers of TiO_2 for the SM pre-treated with thermal treatment and thermal + chemical treatment is presented in Figure 3.2. From this, it is possible to see that the appearance of the layers deposited after each of the pre-treatments is different, with the accumulation of more catalyst along the edges of the SM thermally pre-treated.

After thermal pre-treatment **After 3 layers with T pre-treatment** **After 3 layers with T+C pre-treatment**

Figure 3.2 – Kenics® SM appearance after thermal pre-treatment and after the application of 3 layers to pre-treated SM with thermal (T) treatment or thermal + chemical (T+C) treatment.

For each pre-treatment, 3 replicates were made (Figure 3.3 and Table 3.1) in order to examine the reusability of the deposited film. Replicates showed similar BrO_3^- reductions, indicating no deterioration of the film deposited.

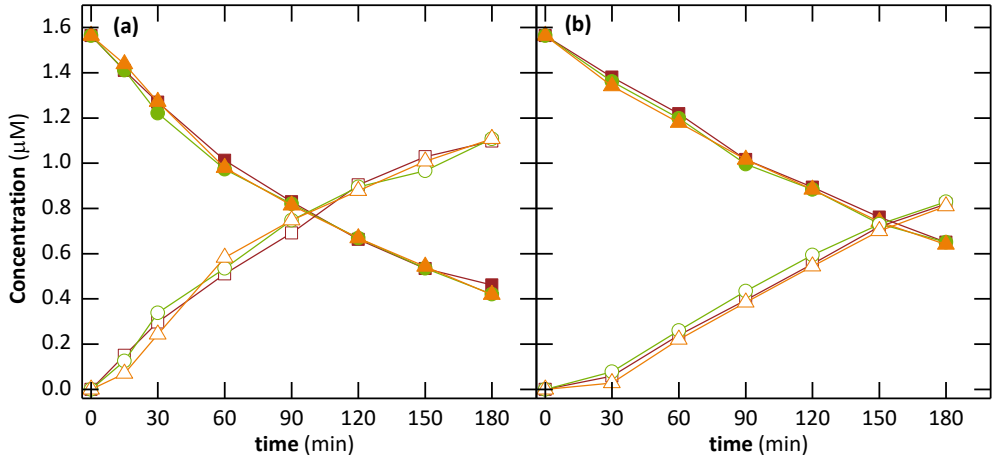

Figure 3.3 – Replicates of TiO_2 PC applied to BrO_3^- reduction using different SM pre-treatments. Solid symbols: BrO_3^- concentration. Open symbols: Br^- concentration. SM pre-treatment: thermal (a), thermal + chemical (b). Replicates: 1st (■,□), 2nd (●,○), 3rd (▲,△). Conditions: $[BrO_3^-]_0$: 1.56 μM; SM position during dip-coating: Vertical; Number of layers: 3; pH: 5.5; [DO]: 212-239 μM; Simulated sunlight; *T*: 25 ºC; *Q*: 50 L h^{-1}.

Figure 3.4 and Table 3.1 exhibit the comparison between the applications of thermal + chemical pre-treatment and thermal treatment only. Simple thermal treatment was better than using thermal and chemical treatments in sequence, allowing the reduction reaction to proceed faster (33% higher $k_{bromate}$), originating higher concentrations of Br^-. Under the operational conditions used, almost all the added BrO_3^- was converted to Br^- with no identification of intermediary compounds. The same applies to the rest of the results obtained in this dissertation.

Taking into account these results and the appearance of the SM previously described, it can be suggested the occurrence of distinct modifications on the SM surface during the thermal + chemical pre-treatment when compared to the thermal one. The TiO_2 films produced for both pre-treatments can be further characterized in terms of morphological properties, as also proposed in *section 5*. Montecchio et al. [75] evaluated the effect of different surface treatments on stainless steel. The treatment with sulfuric acid (30 wt. %) lead to high degrees of surface modification only at the nano-scale level. This have led to low photocatalytic performances, the lowest when compared to the other treatments made, because the larger powder agglomerates were exposed and quickly detached from the support and only the finer particles were protected as a result of a rougher nano-scale structure. Moreover, the used Kenics® SM in this dissertation was mainly composed of chromium and iron, which can be dissolved to their respective ions in the presence of sulfuric acid [75,76]. As a result, the surface of the SM is highly affected by the acid used.

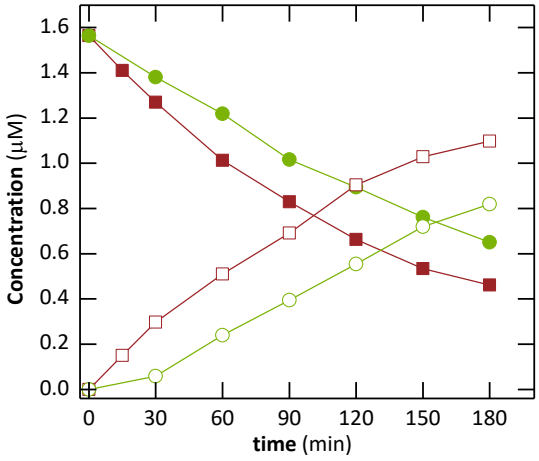

Figure 3.4 - Influence of SM pre-treatment on BrO_3^- reduction by TiO_2 PC. Solid symbols: BrO_3^-concentration. Open symbols: Br^- concentration. SM pre-treatment: thermal (■,□), thermal + chemical (●,○). Conditions: $[BrO_3^-]_0$: 1.56 μM; SM position during dip-coating: Vertical; Number of layers: 3; pH: 5.5; [DO]: 212-239 μM; Simulated sunlight; *T*: 25 ºC; *Q*: 50 L h^{-1}. 1st replicate of each condition was used.

Based on these results, the thermal SM pre-treatment was selected for all subsequent trials. All these trials were performed in duplicate or triplicate. For some conditions, the triplicates results are presented. After four reactions using the same photocatalytic TiO_2 film, an initial reaction was replicated. The same TiO_2 film was used for a maximum of twelve consecutive reactions. The reactions could be always reproduced, thereby pointing to a very good adherence and stability of the TiO_2 films deposited by dip-coating on the stainless steel surface of the SM. It is likely that the TiO_2 films can be stable for more than twelve usages.

.

3.3. Influence of number of layers deposited on the static mixer by dip-coating

TiO_2 dosage coated on the SM was evaluated in terms of the number of layers (1, 3, 6 and 12), being represented in Figure 3.5 the appearance of the SM after each deposition approach. As it is possible to visualize, higher PCT accumulations occur for increasing number of layers mostly along the edges surface of the SM, being represented with enhancing color. This occurs possibly as a result of the position of the SM (vertical) that facilitates deposition on its side surfaces.

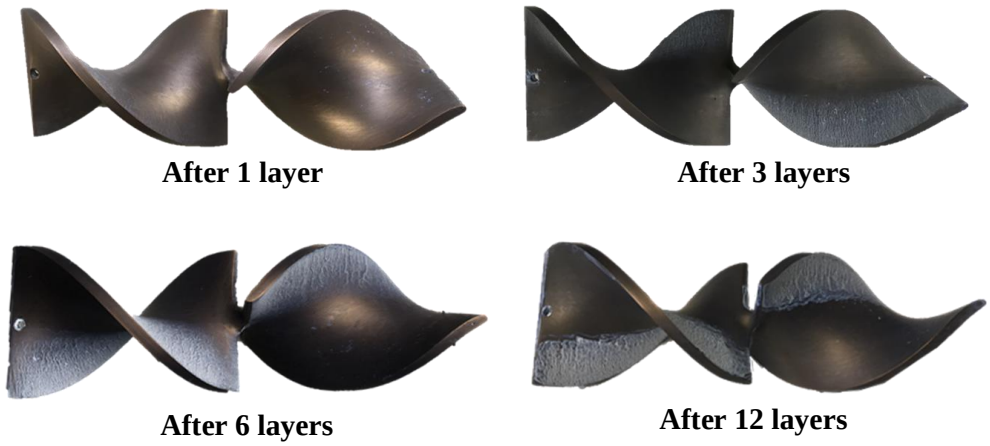

Figure 3.5 - Kenics® SM appearance after 1, 3, 6 and 12 layers.

For each number of the layers, 3 replicates were conducted – see Figure 3.3b for 3 layers, Figure 3.6 for 1, 6 and 12 layers, and Table 3.1 for the $k_{bromate}$ of all reactions. The results reveal reusability of the SM for all TiO_2 dosages, with no deterioration of the PCT films.

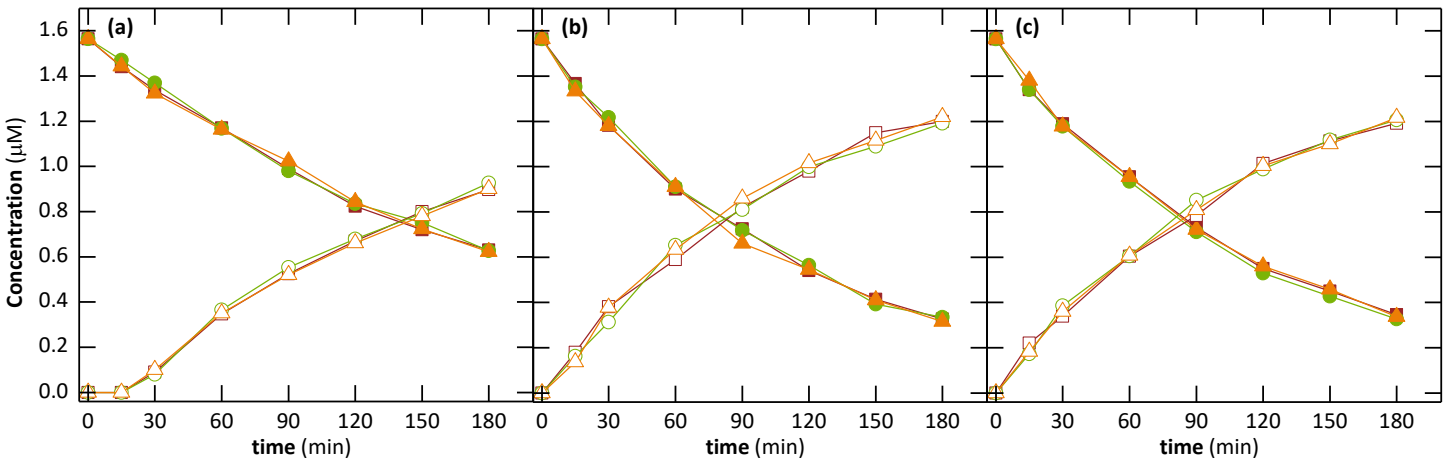

Figure 3.6 - Replicates of TiO_2 PC applied to BrO_3^- reduction using SM with different number of layers deposited by dip-coating. Solid symbols: BrO_3^- concentration. Open symbols: Br^- concentration. Number of layers: 1 (a), 6 (b), 12 (c) (replicates of 3 layers are represented in Figure 3.3b). Replicates: 1st (■,□), 2nd (●,○), 3rd (▲,△). Conditions: $[BrO_3^-]_0$: 1.56 μM; SM pre-treatment: Thermal; SM position during dip-coating: Vertical; pH: 5.5; [DO]: 212-239 μM; Simulated sunlight; *T*: 25 ºC; *Q*: 50 L h^{-1}.

The effects of the different TiO_2-P25 layers on the reduction kinetics of BrO_3^- are presented in Figure 3.7 and Table 3.1. Higher BrO_3^- reductions were achieved for increasing number of layers up to 6, with similar results for 6 and 12 layers. This is typical of a true heterogeneous catalytic system, where the amount of compound reduction increases with increasing the PCT dose [28]. The results obtained indicate improved absorption of incoming photons for ticker TiO_2 films up to a given thickness, corresponding to the deposition of 6 layers, for which occurred the complete absorption of photons potentially absorbable by the PCT. From 6 to 12 layers the diffusional length of e^-/h^+ pairs to the catalyst-liquid interface remained unaffected.

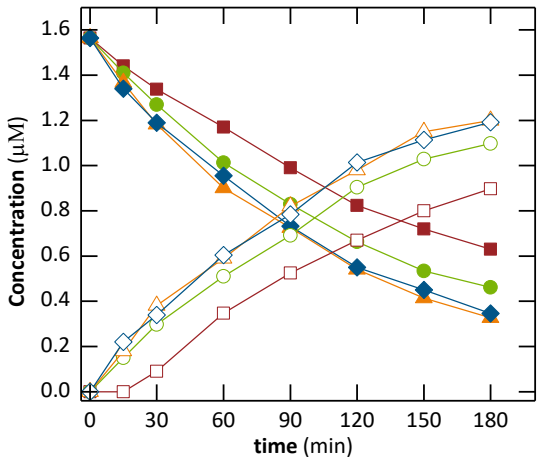

Figure 3.7 - Influence of number of layers deposited on the SM by dip-coating on BrO_3^- reduction by TiO_2 PC. Solid symbols: BrO_3^- concentration. Open symbols: Br^- concentration. Number of layers: 1 (■,□), 3 (●,○), 6 (▲,△), 12 (◆,◇). Conditions: $[BrO_3^-]_0$: 1.56 μM; SM pre-treatment: Thermal; SM position during dip-coating: Vertical; pH: 5.5; 1st Replicate; [DO]: 212-239 μM; Simulated sunlight; *T*: 25 ºC; *Q*: 50 L h^{-1}. 1st replicate of each condition was applied.

These results allowed to determine the optimum catalyst loading that permitted to ensure total absorption of efficient photons and the highest BrO_3^- removal with the minimum amount of PCT used. Hence, 6 was the number of TiO_2 layers considered as optimum and used in the subsequent experiments.

Furthermore, dark experiments were carried out for each number of layers under the same operational conditions applied in the photocatalytic trials (Figure 3.8). The aim was to assess the extent of BrO_3^- adsorption on the PCT surface. The results obtained show negligible BrO_3^- concentration decay variation (< 5%) and, consequently, no obvious adsorption.

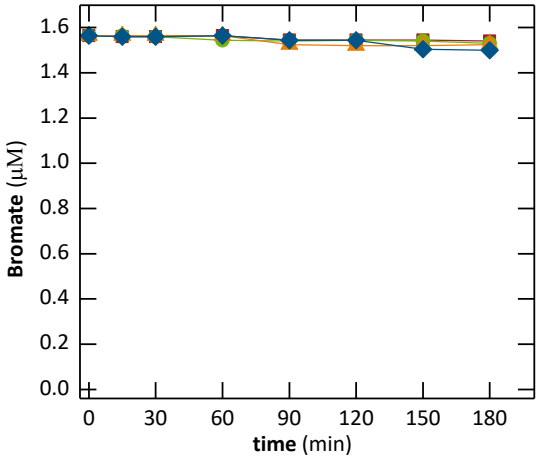

Figure 3.8 - Adsorption of BrO_3^- on the TiO_2 PCT assessed by recirculating the BrO_3^- solution in the dark using the SM coated with different number of layers: 1 (■), 3 (●), 6 (▲), 12 (◆). Conditions: $[BrO_3^-]_0$: 1.56 μM; SM pre-treatment: Thermal; SM position during dip-coating: Vertical; pH: 5.5; [DO]: 212-239 μM; Simulated sunlight; *T*: 25 ºC; *Q*: 50 L h^{-1}.

3.4. Influence of static mixer position during dip-coating

As explained before and considering Figure 2.2, the dip-coating procedure on the Kenics® SM was done vertically and horizontally. Figure 3.9 presents the appearance of the SM after 6 layers deposition for each position. Observing the figure, it is possible to see that film homogeneity seemed better for the horizontal deposition, because less accumulation of PCT particles on surface sides was presented.

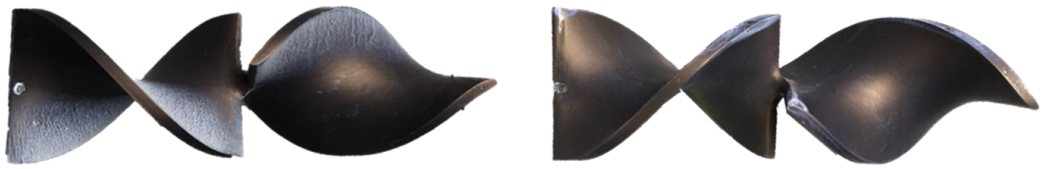

Vertical **Horizontal**

Figure 3.9 – Kenics® SM appearance after 6 layers deposition according to the position: vertical (left), and horizontal (right).

Because film homogeneity commonly has a positive effect on coating adherence, it would be expected for horizontal deposited layers to present better results. In order to evaluate films reusability, 3 replicates were conducted for each of the positions. The results are presented in Figure 3.6b (for vertical deposition) and Figure 3.10 (for horizontal deposition), and Table 3.1. Reusability of PCT films was proved for both dip-coating positions, with no TiO_2 particles detachment occurring despite the poorer film homogeneity attained for the vertical deposition. According to Vásquez et al. [72], higher film homogeneities mean higher consolidation of the PCT particles, resulting in greater integrity and stability of the film, improving also the coating adherence on the supports. This means that with more homogeneous films, less PCT particles release from the support. As a result, it would be expected particles detachment in the case of vertical film deposition, which did not occur.

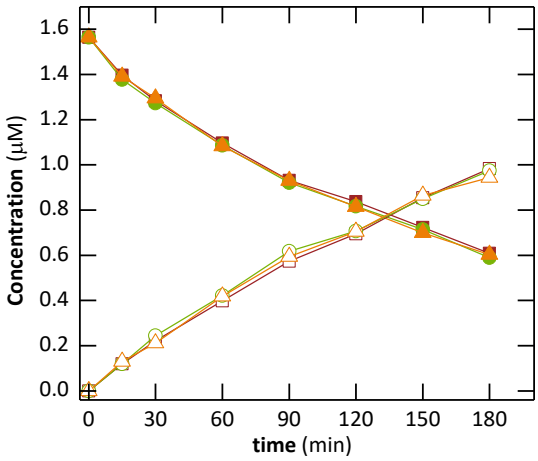

Figure 3.10 - Replicates of TiO_2 PC applied to BrO_3^- reduction using SM in horizontal position during dip-coating. Solid symbols: BrO_3^- concentration. Open symbols: Br^- concentration. Replicates: 1st (■,□), 2nd (●,○), 3rd (▲,△). Conditions: $[BrO_3^-]_0$: 1.56 µM; SM pre-treatment: Thermal; Number of layers: 6; pH: 5.5; [DO]: 212-239 µM; Simulated sunlight; *T*: 25 ºC; *Q*: 50 L h^{-1}.

Figure 3.11 and Table 3.1 show the comparison between the effects of the two positions during dip-coating on BrO_3^- removal. The results obtained showed greater reduction efficiencies for vertical deposition rather than horizontal: 76% *versus* 61% reduction after 180 min of reaction, and a $k_{bromate}$ 39% higher. This means that greater homogeneities not always result in higher efficiencies. In fact, the ticker films near the edges of the SM may have improved the photocatalytic activity.

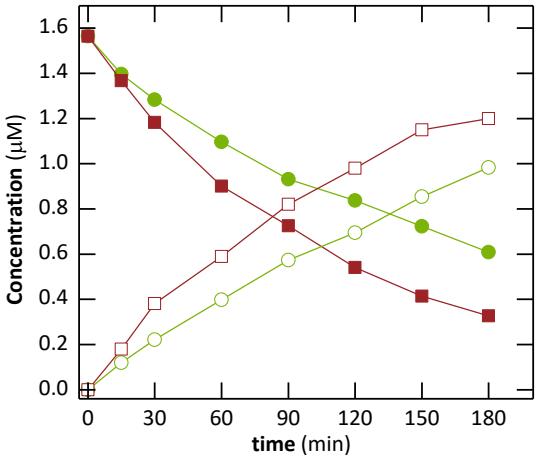

Figure 3.11 - Influence of SM position during dip-coating on BrO_3^- reduction by TiO_2 PC. Solid symbols: BrO_3^- concentration. Open symbols: Br^- concentration. SM position during dip-coating: vertical (■,□), horizontal (●,○). Conditions: $[BrO_3^-]_0$: 1.56 μM; SM pre-treatment: Thermal; Number of layers: 6; pH: 5.5; [DO]: 212-239 μM; Simulated sunlight; *T*: 25 ºC; *Q*: 50 L h^{-1}. 1st replicate of each condition was applied.

Taking into account the aforementioned results, for the subsequent experiments the deposition of the 6 PCT layers was done with the SM in the vertical position.

3.5. Influence of pH

Although Zhang et al. [52] determined that pH 5.5 was the optimum pH for the TiO_2-P25 PC applied to BrO_3^- removal, it is important to study the influence of pH in our system. Consequently, other four pH were tested: two acidic ones (3.0 and 4.0) and two pH in agreement with the requirements for drinking water (6.5 and 7.0) [17,77]. Figure 3.12 and Table 3.1 presents the comparison between the five pH values tested.

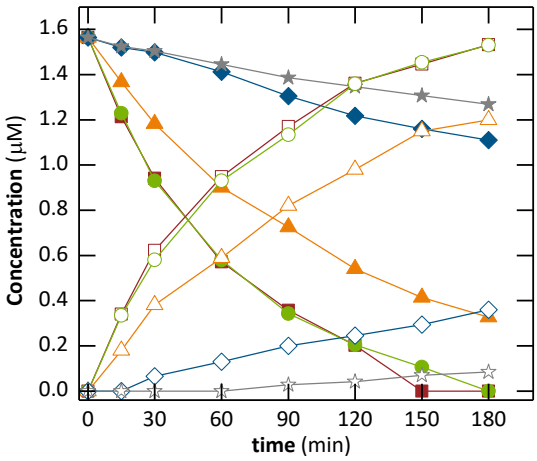

Figure 3.12 - Influence of pH on BrO_3^- reduction by TiO_2 PC. Solid symbols: BrO_3^- concentration. Open symbols: Br^- concentration. pH: 3.0 (■,□), 4.0 (●,○), 5.5 (▲,△), 6.5 (◆,◇), 7.0 (★,☆). Conditions: $[BrO_3^-]_0$: 1.56 μM; SM pre-treatment: Thermal; SM position during dip-coating: Vertical; Number of layers: 6; [DO]: 212-239 μM; Simulated sunlight; *T*: 25 ºC; *Q*: 50 L h^{-1}. 1st replicate of each condition was applied.

BrO_3^- reduction decreased with increasing pH. Complete and quite similar BrO_3^- reductions were achieved for both pH 3.0 and 4.0, with the major differences at the reaction end with total BrO_3^- reduction after 150 min and 180 min, respectively. 79%, 29% and 19% BrO_3^- reduction was attained for pH 5.5, 6.5 and 7.0, respectively, after 180 min of reaction. The PZC for TiO_2-P25 is in the range of 6.2-6.4 [24,50–52], which means that its surface is negatively charged at pH>6.2-6.4 and positively charged at pH<6.2-6.4 (Eqs. 13 and 14). Because at pH 6.5 and 7.0 the TiO_2 surface is negatively charged, a repulsion between the PCT and BrO_3^- may have occurred, decreasing reaction kinetics. O_2 reduction by e^- is then likely to take place instead of BrO_3^- reduction. At pH 3.0, 4.0 and 5.5, the surface is positively charged, attracting BrO_3^- and increasing reaction kinetics.

Furthermore, pH also influences the potential of VB and CB of TiO_2, as can be seen in Figure 3.13, with the potential of both e^- and h^+ going to more negative values with pH increase. Also, the BrO_3^- potential is affected by pH, showing lower values for higher pH (see Table 3.2). The more negative values for higher pH presented in Figure 3.13 means that TiO_2 has a stronger reduction potential, which would improve the reaction if BrO_3^- potentials were independent of pH. However, BrO_3^- and TiO_2 potentials decreased at the same rate for rising pH, pointing to a constant difference between the TiO_2 CB and BrO_3^- potentials for all pH values. Thus, the effect of pH on TiO_2 and BrO_3^- redox potential might not have affected the process efficiency, being BrO_3^- reduction mainly affected by the charge of TiO_2.

Similar results have been reported by Noguchi et al. [68], where TiO_2 ST-21 was used as the PCT to study the influence of pH and surface charge on BrO_3^- reduction. A summary of the operational parameters used is presented in Table 1.2. The group concluded that the BrO_3^- reduction rate was highly sensitive to pH, increasing with pH decreasing: higher BrO_3^- reduction and adsorption followed the order of pH 5.0> 5.5> 6.0> 6.5> 7.0. This occurred because with pH declining, the adsorbed amounts of BrO_3^- increase, suggesting that the ion is predominantly adsorbed on positively charged surfaces in order to promote the photocatalytic reduction. On the other hand, Zhang et al. [52] have concluded that BrO_3^- reduction rate was higher for pH 5.5 than for pH 3.0. These results were explained by the authors as related to another possible route of pH influence on the photocatalytic reduction of BrO_3^-, rather than the one described earlier.

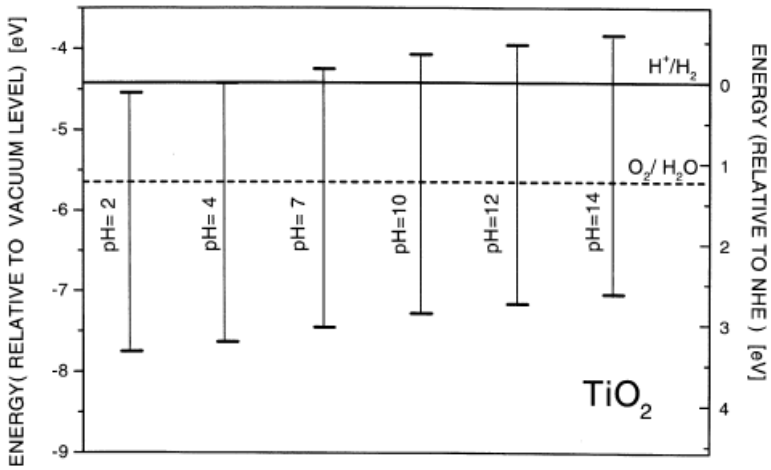

Figure 3.13 – Effect of pH on energy of TiO_2 in terms of vacuum level and normal hydrogen electrode level in electrolyte. Adapted from Bak et al. [78], Copyright © (2002), with permission from Elsevier.

Table 3.2 - BrO_3^- redox potentials according to pH.

pH	E_0 (BrO_3^-/Br^-) (V)
3.0	1.25
4.0	1.19
5.5	1.10
6.5	1.04
7.0	1.01

3.6. Influence of dissolved oxygen content

Because the DO in aqueous solutions has a significant influence in PC, having an effective role in pollutants redox reactions, it is important to assess its effects on the BrO_3^- reduction according to the different pH tested. Therefore, experiments were conducted with air (21% O_2) and purged N_2 (limited O_2). Figure 3.14 and Table 3.1 display the DO effects on BrO_3^- reduction at various solution pH. Figure 3.15 shows the amount of DO during the experiments of Figure 3.14 in the absence of N_2, where DO varied between 212 and 239 µM. In the presence of N_2, the DO contents were always below 3.1 µM, corresponding to the detection limit of the DO analyzers.

According to some authors [51,53,54], DO is usually not desired in the photoreduction because it competes for the photogenerated e^- with the substrate. However, in the current study this was only observed for pH 6.5 and 7.0. At pH 6.5, the negative influence of DO on BrO_3^- reduction was maximum, with the $k_{bromate}$ being 42% lower in the absence of N_2 supply. At pH 7.0, the negative influence of DO on BrO_3^- reduction was observed in lower extent than at pH 6.5. The difference between pH 6.5 and 7.0 can be explained by the more repulsion between TiO_2 and BrO_3^- that occur for pH 7.0 because it is distant from the PZC of the PCT. Even in the presence of more e^- (lower DO contents), repulsion still prevails and the photoreduction process continues to be better for pH 6.5. At pH 3.0, 4.0 and 5.5, the efficiency of BrO_3^- reduction was quite similar for both DO ranges. These results can be attributed to a stronger adsorption of BrO_3^- onto the TiO_2 surface at pH values below 6.2-6.4, i.e. the PZC of TiO_2-P25 [24,50–52], with DO having more difficulty to take e^- for its reduction. At pH values above 6.2-6.4, the BrO_3^- adsorption onto the TiO_2 surface was weaker and so the DO took advantage from the BrO_3^- in the competition for e^-.

Despite the better results at pH 6.5 and 7.0 in the presence of N_2 supply, it is important to notice that the highest reductions obtained at these pH values were not as high as the ones obtained for pH 5.5, 4.0 and 3.0.

Ku and Jung [79] have concluded that for the photocatalytic reduction of Cr (VI) by TiO_2/UV, the DO present at acidic pH had little influence but at alkaline values it decreased the process. This was attributed to the fact that at alkaline pH, the DO might compete more favorably with Cr (VI) for e^- than it competed at acidic pH. These conclusions are in agreement with the ones found in this dissertation.

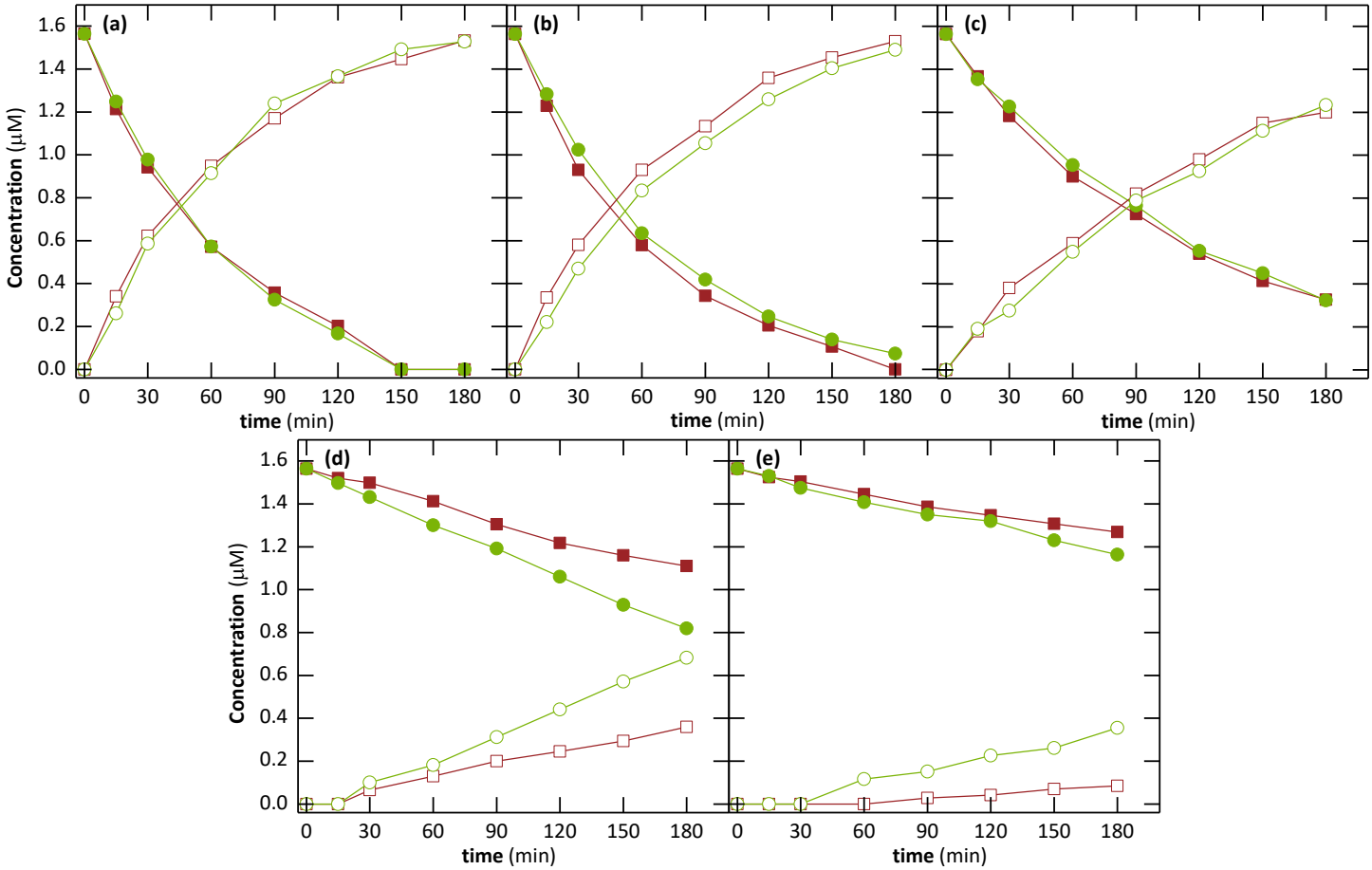

Figure 3.14 - Influence of DO content on BrO_3^- reduction by TiO_2 at various pH values: 3.0 (a), 4.0 (b), 5.5 (c), 6.5 (d), 7.0 (e). Solid symbols: BrO_3^- concentration. Open symbols: Br^- concentration. [DO]: 212-239 μM (absence of N_2) (■,□), <3.1 μM (presence of N_2) (●,○). Conditions: $[BrO_3^-]_0$: 1.56 μM; SM pre-treatment: Thermal; SM position during dip-coating: Vertical; Number of layers: 6; Simulated sunlight; *T*: 25 ºC; *Q*: 50 L h^{-1}. 1st replicate of each condition was applied.

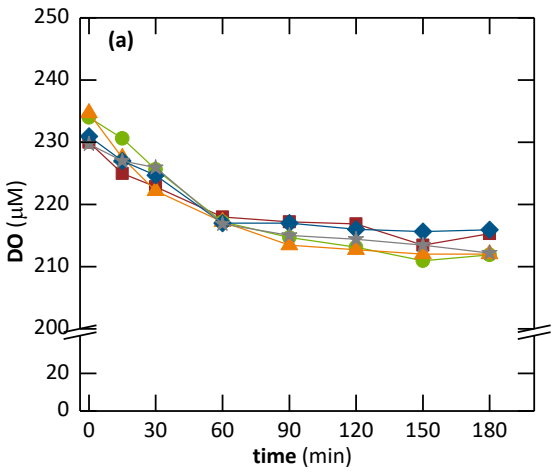

Figure 3.15 - DO content for TiO_2 photocatalytic experiments of Figure 3.14 in the absence of N_2. pH: 3.0 (■), 4.0 (●), 5.5 (▲), 6.5 (◆), 7.0 (★).

3.7. Influence of the addition of an organic sacrificial agent – Formic acid

As stated in *section 1.2*, organic compounds are often added as SAs in photocatalytic reductions in order to: (i) generate strong reducing species via Eq. (10), (ii) minimize the recombination of e^-/h^+ pairs due to the oxidation of the SAs by h^+ or $HO^\bullet$ via Eq. (9), and (iii) minimize species reoxidation via Eq. (8) since the h^+ or $HO^\bullet$ are used to oxidize the SA via Eq. (9) [36]. According to Tan et al. [53] and Dionysiou et al. [36], an effective organic SA must be able to adsorb on the PCT surface, be easily mineralized, and have the ability to form strong reducing species. HCOOH has been indicated as one of the best organic SAs for photocatalytic reductions. Nguyen et al. [80] studied the effect of methanol and HCOOH on the photocatalytic reduction of cadmium (Cd) using TiO_2 as a PCT, at pH 7.0 and with N_2 supply. In the absence of methanol and HCOOH, little Cd ($[Cd]_0$: 30 ppm) was removed from the solution, and by adding methanol no Cd reduction occurred. On the contrary, upon the addition of HCOOH, a substantial removal of Cd was observed, which increased with increasing HCOOH concentrations from 10 to 300 ppmC (molar ratio of ca. 1:1 to 25:1). A further increase to 600 ppmC (ca. 50:1 molar ratio) did not improve removal. Tan et al. [53] studied the effect of three organic compounds (HCOOH, methanol and ethanol) on the photocatalytic reduction (TiO_2/UV) of selenium (Se) anions at acidic pH (3.0). After 120 min of irradiation, the highest amount of Se(IV) and Se(VI) removed from the system occurred when HCOOH was present. Also, HCOOH was the organic compound that adsorbed the most to TiO_2 surface and the presence of methanol and ethanol enabled the reduction of Se(IV) and Se(VI). As a result, HCOOH was determined the best organic additive because it achieved the most efficient reductions. Both studies concluded that the efficient photoreduction of HCOOH was due to (i) its ability of being adsorbed onto the TiO_2 surface, (ii) it can efficiently form strong reducing radicals, namely $CO_2^{-\bullet}$, as a result of $HO^\bullet$ trapping, and (iii) its ease of mineralization to CO_2. In a subsequent study, Tan an co-workers [54] concluded that the adsorption of Se(VI) and HCOOH on the TiO_2 surface was essential for the photoreduction of the metal to take place. Also, they determined that the optimum photoreduction rate was close to the correlated ratio of molar adsorption (3:1), demonstrating that redox reactions take place on the surface of the PCT, in which the adsorption surface sites are limited. Similarly, Marks et al. [81] studied the TiO_2/UV reduction of oxoanions (including BrO_3^-) under the addition of HCOOH at neutral and acidic pH. The HCOOH concentration added to the system was determined in the basis of stoichiometry. For BrO_3^-, the group concluded that the theoretical HCOOH:BrO_3^- molar ratio was 3:1. In the experimental procedure, they observed a ratio of 2.91:1. The results obtained in this work showed that BrO_3^- was the only compound with measurable photocatalytic reduction at both pH conditions. However, its reduction rate was extremely slow in the absence of HCOOH, meaning that in order to improve process efficiency the addition of an organic compound is imperative.

Once the future scope is to apply the process studied in this dissertation in real conditions, the pH 6.5, i.e. the minimum pH for drinking water [17,77] was selected to assess the influence of organic SA. It is important to check if it is possible to improve BrO_3^- reduction kinetic rate at this pH. Working in real conditions at acidic pH, as is the case of pH 3.0 and 4.0 for which the BrO_3^- reduction was maximum (*section 3.5*), would imply higher operational costs in order to (i) decrease the untreated water pH, and (ii) increasing it again after treatment to a value equal or greater than 6.5, so it can be under the limits implemented [17,77].

Simultaneously with the application of pH 6.5, the optimum conditions obtained so far were implemented: thermal SM pre-treatment, 6 layers, vertical position of SM during dip-coating

and presence of N_2 to lower DO contents in the system. In order to improve process efficiency, the addition of HCOOH was studied. To do so, a molar fraction of 3:1 was firstly tested, as it was determined by Marks et al. [81] as the theoretical ratio required. Besides this used HCOOH:BrO_3^- molar ratio, others were also applied, as 1:1 and 0.5:1 ratios. Results of the effect of HCOOH addition on BrO_3^- reduction are shown in Figure 3.16 and Table 3.1.

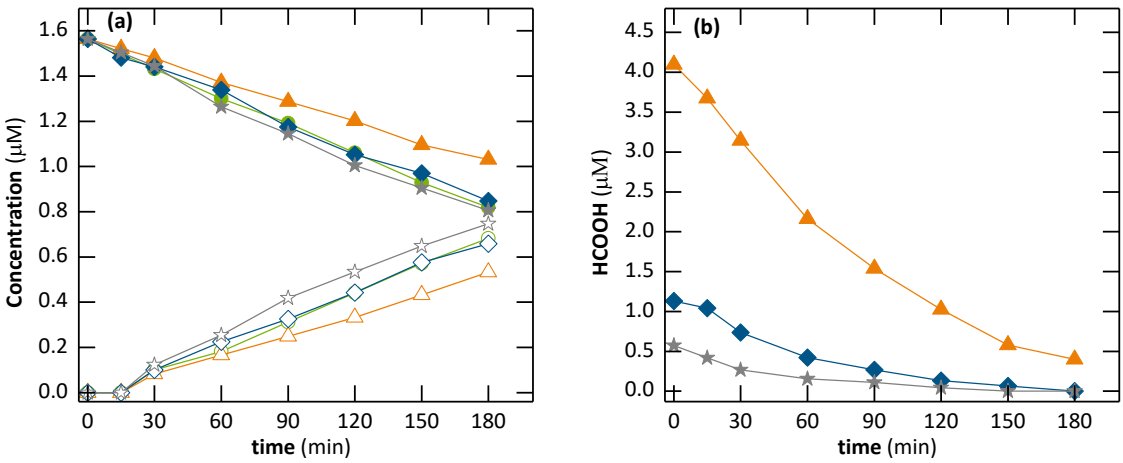

Figure 3.16 - Influence of addition of different contents of HCOOH at pH 6.5 for [DO] <3.1 μM (presence of N_2) on BrO_3^- reduction by TiO_2 PC in terms of BrO_3^- concentration (solid symbols) and Br^- concentration (open symbols) (a), and HCOOH[a] concentration (b). HCOOH:BrO_3^- molar ratio: absence of HCOOH addition (●,○), 3:1 (▲,△), 1:1 (◆,◇), 0.5:1 (★,☆). Conditions: $[BrO_3^-]_0$: 1.56 μM; SM pre-treatment: Thermal; SM position during dip-coating: Vertical; Number of layers: 6; Simulated sunlight; *T*: 25 ºC; *Q*: 50 L h^{-1}. 1st replicate of each condition was applied.
[a] Detection of $HCOO^-$ by ion chromatography.

The results obtained using a HCOOH:BrO_3^- molar ratio of 3:1 show a decrease of the photocatalytic reduction process when compared with the reaction with no HCOOH addition (from 48% BrO_3^- removal to 34% after 180 min of reaction). For HCOOH:BrO_3^- molar ratios of 1:1 and 0.5:1 null improvement of the photoreduction occurred.

The decrease of the photocatalytic reduction using a HCOOH:BrO_3^- molar ratio of 3:1 might be related with an excess of HCOOH, which can saturate the TiO_2 surface and hinder BrO_3^- reduction. Note that HCOOH only absorbs radiation for wavelengths below ≈250 nm (results not shown), being unable to absorb the photons emitted by the simulated sunlight (wavelengths ranging from 280 to 400 nm).

For HCOOH:BrO_3^- molar ratios of 1:1 and 0.5:1, the saturation of the TiO_2 surface with HCOOH should not have occurred. Nevertheless, BrO_3^- reduction was unable to be enhanced by the strong reducing species $CO_2^{-\bullet}$, formed via Eq. (10), neither by the availability of more e^- due to the minimization of the recombination of e^-/h^+ pairs or the minimization of Br^- reoxidation to BrO_3^-. It is likely that the null improvements on BrO_3^- reduction for HCOOH:BrO_3^- molar ratios of 1:1 and 0.5:1 can be associated with the weak adsorption of BrO_3^- onto TiO_2 surface that occur at pH 6.5. At this pH, the TiO_2 surface is expected to be slightly negative/almost neutral, considering that the PZC for TiO_2 is in the range of 6.2-6.4 [24,50–52].

It is worth mentioning that the ratio of HCOOH:BrO_3^- was not kept constant during the reaction since the decay of HCOOH and BrO_3^- did not follow the same trend. Furthermore, the HCOOH consumption was higher and faster for increasing concentrations, as it can be noticed from the steep line respecting HCOOH at 3:1 ratio. For 0.5:1 and 1:1 ratios, HCOOH was totally consumed.

Moreover, it was assessed if the same results would prevail in the presence of high amounts of DO (212-239 µM). To do so, experiments with the addition of HCOOH:BrO_3^- molar ratios of 3:1 and 0.5:1 were carried out and compared with the reaction where no HCOOH was added. The results are shown in Figure 3.17.

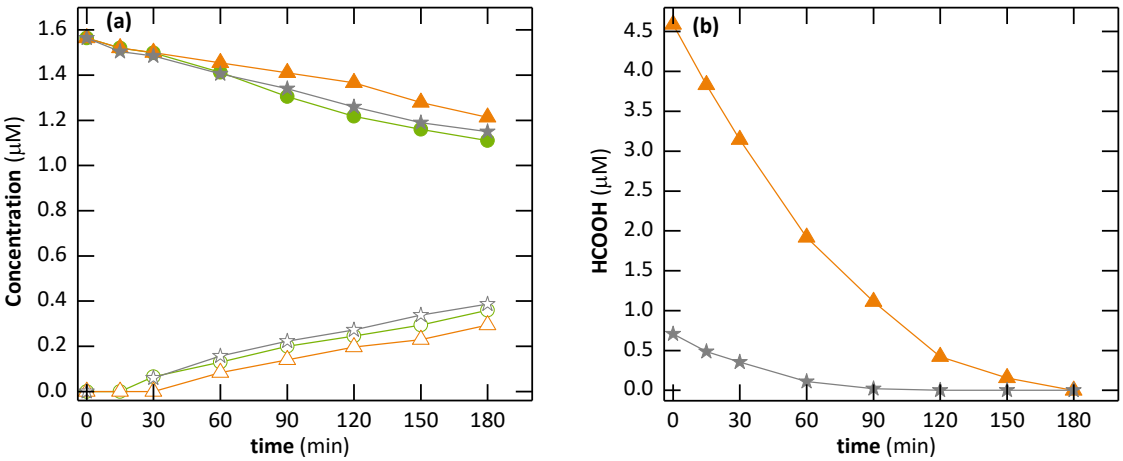

Figure 3.17 - Influence of the addition of different contents of HCOOH at pH 6.5 for [DO] of 212-239 µM (absence of N_2) on BrO_3^- reduction by TiO_2 PC in terms of BrO_3^- concentration (solid symbols) and Br^- concentration (open symbols) (a), and HCOOH[a] concentration (b). HCOOH:BrO_3^- molar ratio: absence of HCOOH addition (●,○), 3:1 (▲,△), 0.5:1 (★,☆). Conditions: $[BrO_3^-]_0$: 1.56 µM; SM pre-treatment: Thermal; SM position during dip-coating: Vertical; Number of layers: 6; Simulated sunlight; *T*: 25 ºC; *Q*: 50 L h^{-1}. 1st replicate of each condition was applied.
[a] Detection of $HCOO^-$ by ion chromatography.

Similarly to what happened when N_2 was present, no significant differences were obtained for BrO_3^- photoreduction in the absence and presence of HCOOH. For 212-239 µM of DO, the amounts of e^- at the TiO_2 surface that are able to reduce BrO_3^- might be lower compared to the ones registered when N_2 was supplied since the DO also reacts with e^-. The presence of HCOOH might have improved the amount of e^- due the minimization of e^-/h^+ pairs recombination, however, it is likely that the weak adsorption of BrO_3^- that occur at pH 6.5 did not allow to take advantage of this higher availability of e^-.

Once again, molar ratios were not kept during the experiments since BrO_3^- and HCOOH were not removed with the same rates.

Moreover, the recirculation of the aqueous BrO_3^- + HCOOH solutions in the system with no light before the reaction start (solution homogenization) led to null/almost HCOOH adsorption onto the TiO_2 surface when high DO contents were present (Figure 3.17b), which contrasts with the HCOOH adsorptions achieved in the presence of null/almost null DO contents (Figure 3.16b).

For the 3:1 HCOOH:BrO_3^- molar ratio, the HCOOH content decayed from ca. 4.69 µM to 4.59 µM and 4.10 µM in the presence and absence of high DO contents, respectively. For the 0.5:1 HCOOH:BrO_3^- molar ratio, the HCOOH content decreased from ca. 0.78 µM to 0.71 µM and 0.57 µM in the presence and absence of high DO contents, respectively. These results suggest that the presence of high levels of DO can saturate the PCT surface, reducing HCOOH adsorption. When DO levels were null/almost null, HCOOH could be more strongly adsorbed onto TiO_2 because no DO was blocking its surface.

As can be seen in Figure 3.16b and Figure 3.17b, the HCOOH reduction kinetic rates were higher for experiments in the presence of high DO amounts. This can be attributed to the occurrence of e^-/h^+ pairs recombination in lower extent in the presence of high contents of DO since this species react with e^-, with consequent increment of the number h^+ and $HO^\bullet$ to oxidize the HCOOH.

The results obtained in this section permit to determine that at pH 6.5, the minimum pH acceptable for drinking water, it is preferable to work under limited levels of DO and in the absence of an organic SA in order to achieve a good BrO_3^- photoreduction.

4. CONCLUSIONS

A Kenics® SM was successfully applied as a TiO_2-P25 support for the photocatalytic reduction of BrO_3^- in aqueous solution carried out in a tubular photoreactor with CPCs. This photocatalytic system reduced mass transfer limitations by enhancing the diffusion of BrO_3^- to the liquid-PCT interface and to the active surface sites inside the PCT film, and reduced photon transfer limitations by increasing illumination efficiency since the entire surface of the TiO_2 film was receiving front side illumination. The TiO_2-P25 films deposited on the SM surface by dip-coating technique proved to have high adherence and stability, allowing the replication of BrO_3^- photoreduction kinetics over at least twelve usages. Total or almost total BrO_3^- reduction into Br^- was always achieved, without the identification of intermediates.

Considering the influence of various operational variables on the BrO_3^- photocatalytic reduction, the following conclusions were extracted: (i) the application of a thermal treatment to the SM before TiO_2 deposition led to a higher photoreduction efficiency than the use of a thermal treatment followed by a chemical (acid) treatment, pointing to the formation of better photocatalytic films in the absence of the chemical treatment; (ii) increasing the number of TiO_2 layers deposited by dip-coating only improved the process until a certain value - 6 layers - for which occurred the maximum absorption of photons by the TiO_2; (iii) the position of the SM during the dip-coating procedure proved to have influence on the BrO_3^- photoreduction, being preferable to coat it in the vertical position probably due to the formation of a ticker layer near the edges of the SM; (iv) the BrO_3^- photoreduction increased for lower pH values from 7.0 to 4.0, which can be mainly attributed to the positive charge of the TiO_2 surface at pH below the PZC for TiO_2-P25, i.e. 6.2-6.4 [24,50–52], attracting BrO_3^- and increasing reaction kinetics; (v) high levels of DO present in the solution proved to be negative for pH 6.5 and 7.0, and had a negligible effect at pH 3.0, 4.0 and 5.5, which can be mainly attributed to a weaker adsorption of BrO_3^- onto the TiO_2 surface at pH values above 6.2-6.4, with consequent higher competition of DO with BrO_3^- for e^-; and (vi) using HCOOH as an organic SA at pH 6.5 did not improve BrO_3^- photoreduction either in the presence or absence of high levels of DO, suggesting that the weak adsorption of BrO_3^- onto TiO_2 surface that occur at pH 6.5 did not allow to take advantage of $CO_2^{-\bullet}$ formation, higher amounts of e^- and lower susceptibility of Br^- reoxidation to BrO_3^- that occur in the presence of HCOOH.

5. SUGGESTIONS FOR FUTURE WORK

Since the BrO_3^- photocatalytic reduction at pH 6.5 in the presence of HCOOH presented a small rate, it would be interesting to test other proven efficient organic SA, such as methanol, ethanol, EDTA and citric acid, and also the influence of organic SA at acidic pH values.

Taking into consideration that temperature can affect e^-/h^+ recombination, the desorption of adsorbed compounds on the TiO_2 surface and the redox potential of species according to the Nernst equation, testing the BrO_3^- photocatalytic reduction at other temperatures from 5 to 40 ºC can be interesting.

Additionally, it would be interesting to assess if the generated species have or not ability to oxidize Br^- to BrO_3^-, as other authors evaluated, at different pH values and DO contents.

Moreover, it is important to characterize the morphological properties of the TiO_2 films synthetized by applying distinct SM pre-treatments (thermal *versus* thermal + chemical), distinct number of layers and the SM in vertical and horizontal positions during the dip-coating procedure. Various imaging and spectroscopy techniques can be employed, including scanning electron microscopy (SEM) coupled with energy dispersive X-ray (EDS) to identify particle features such as the shape and size along with their corresponding distributions in the deposited film.

Because BrO_3^- is present in drinking waters, it would be interesting to study the application of PC to the treatment of real waters resulting from water treatment plants after the application of the ozonation process. Additionally, improving reduction efficiency of this water by changing operational parameters should also be in the scope of future works.

6. REFERENCES

[1] World Health Organization (WHO) (2011). Guidelines for drinking-water quality. 4th edition, Switzerland.

[2] Health Canada (1998). Guidelines for Canadian drinking water quality: Guideline technical document - Bromate.

[3] Health Canada (2010). Screening assessment for the challenge: Bromic acid, potassium salt (Potassium bromate).

[4] Butler, R., Godley, A., Lytton, L., Cartmell, E. (2005). Bromate environmental contamination: Review of impact and possible treatment. *Critical Reviews in Environmental Science and Technology* 35 (3) 193–217.

[5] Pinkernell, U., von Gunten, U. (2001). Bromate minimization during ozonation: Mechanistic considerations. *Environmental Science & Technology* 35 (12) 2525–2531.

[6] Hrubec, J. (Ed.) (1998). Chemistry of aqueous ozone and transformation of pollutants by ozonation and advanced oxidation processes. in *Quality and treatment of drinking water II*, Springer Berlin Heidelberg, Germany.

[7] Antoniou, M., Sichel, C., Andre, K., Andersen, H. R. (2017). Novel pre-treatments to control bromate formation during ozonation. *Journal of Hazardous Materials* 323 (Part A) 452–459.

[8] von Gunten, U. (2003). Ozonation of drinking water: Part II. Disinfection and by-product formation in presence of bromide, iodide or chlorine. *Water Research* 37 (7) 1469–1487.

[9] Antoniou, M. G., Andersen, H. R. (2012). Evaluation of pretreatments for inhibiting bromate formation during ozonation. *Environmental technology* 33 (13–15) 1747–1753.

[10] World Health Organization (WHO) (2010). Bromide in drinking-water. Background document for development of WHO guidelines for drinking-water quality. Switzerland.

[11] Xiao, Q., Yu, S., Li, L., Wang, T., Liao, X., Ye, Y. (2017). An overview of advanced reduction processes for bromate removal from drinking water: Reducing agents, activation methods, applications and mechanisms. *Journal of Hazardous Materials* 324 230–240.

[12] Vainikka, P., Hupa, M. (2012). Review on bromine in solid fuels. Part 1: Natural occurrence. *Fuel* 95 1–14.

[13] International Agency for Research on Cancer (IARC) (1999). IARC monographs on the evaluation of carcinogenic risk to humans: Some chemicals that cause tumours of the kidney or urinary bladder in rodents and some other substances - Potassium bromate.

[14] International Agency for Research on Cancer (IARC) (1986). IARC monographs on the evaluation of the carcinogenic risk of chemicals to humans: Some naturally occurring and synthetic food components, furocoumarins and ultraviolet radiation.

[15] United States Environmental Protection Agency (USEPA) (1998). National primary drinking water regulations: Disinfectants and disinfection byproducts; Final rule. *Public Law* 63 (241) 69390–69476.

[16] United States Environmental Protection Agency (USEPA) (2006). National primary drinking water regulations: Stage 2 disinfectants/disinfection byproducts rule. *Federal Register* 71 (2) 107.

[17] European Communities (1998). Council Directive 98/83/EC of 3 November 1998 on the quality of water intended for human consumption. *Official Journal of the European Communities.*

[18] Portuguese Ministry of Environment (2017). Decree Law 152/2017. *Official Gazette of Portugal, Série I, 235, 2017* 6555–6576.

[19] Mills, A., Belghazi, A., Rodman, D. (1996). Bromate removal from drinking water by semiconductor photocatalysis. *Water Research* 30 (9) 1973–1978.

[20] Hong, S. S., Lee, M. S., Kim, J. H., Ahn, B. H., Lim, K. T., Lee, G. D. (2002). Photocatalytic decomposition of bromate over titanium dioxides prepared using sol-gel method. *Journal of Industrial and Engineering Chemistry* 8 (2d) 150–155.

[21] Mills, A., Le Hunte, S. (1997). An overview of semiconductor photocatalysis. *Journal of Photochemistry and Photobiology A: Chemistry* 108 (1) 1–35.

[22] Gaya, U. I., Abdullah, A. H. (2008). Heterogeneous photocatalytic degradation of organic contaminants over titanium dioxide: A review of fundamentals, progress and problems. *Journal of Photochemistry and Photobiology C: Photochemistry Reviews* 9 (1) 1–12.

[23] Mukherjee, P. S., Ray, A. K. (1999). Major challenges in the design of a large-scale photocatalytic reactor for water tcreatment. *Chemical Engineering & Technology* 22 (3) 253–260.

[24] Coronado, J. M., Fresno, F., Hernández-Alonso, M. D., Portela, R. (Eds.) (2013). Design of advanced photocatalytic materials for energy and environmental applications. Springer London, United Kingdom.

[25] Byrne, C., Subramanian, G., Pillai, S. C. (2017). Recent advances in photocatalysis for environmental applications. *Journal of Environmental Chemical Engineering* (In press).

[26] Ajmal, A., Majeed, I., Malik, R. N., Idriss, H., Nadeem, M. A. (2014). Principles and mechanisms of photocatalytic dye degradation on TiO_2 based photocatalysts: A comparative overview. *RSC Advances* 4 (70) 37003–37026.

[27] Chong, M. N., Jin, B., Chow, C. W. K., Saint, C. (2010). Recent developments in photocatalytic water treatment technology: A review. *Water Research* 44 (10) 2997–3027.

[28] Herrmann, J.-M. (1999). Heterogeneous photocatalysis: Fundamentals and applications to the removal of various types of aqueous pollutants. *Catalysis Today* 53 (1) 115–129.

[29] Yang, J., Dai, J., Chen, C., Zhao, J. (2009). Effects of hydroxyl radicals and oxygen species on the 4-chlorophenol degradation by photoelectrocatalytic reactions with TiO_2-film electrodes. *Journal of Photochemistry and Photobiology A: Chemistry* 208 (1) 66–77.

[30] Daghrir, R., Drogui, P., Robert, D. (2012). Photoelectrocatalytic technologies for environmental applications. *Journal of Photochemistry and Photobiology A: Chemistry* 238 41–52.

[31] Bessegato, G. G., Guaraldo, T. T., de Brito, J. F., Brugnera, M. F., Zanoni, M. V. B. (2015). Achievements and trends in photoelectrocatalysis: From environmental to energy applications. *Electrocatalysis* 6 (5) 415–441.

[32] Pelaez, M., Nolan, N. T., Pillai, S. C., Seery, M. K., Falaras, P., Kontos, A. G., Dunlop, P. S. M., Hamilton, J. W. J., Byrne, J. A., O'Shea, K., Entezari, M. H., Dionysiou, D. D. (2012). A review on the visible light active titanium dioxide photocatalysts for environmental applications. *Applied Catalysis B: Environmental* 125 331–349.

[33] Linsebigler, A. L., Lu, G., Yates, J. T. (1995). Photocatalysis on TiO_2 surfaces: Principles, mechanisms, and selected results. *Chemical Reviews* 95 (3) 735–758.

[34] Oancea, P., Oncescu, T. (2008). The photocatalytic degradation of dichlorvos under solar irradiation. *Journal of Photochemistry and Photobiology A: Chemistry* 199 (1) 8–13.

[35] Verbruggen, S. W. (2015). TiO_2 photocatalysis for the degradation of pollutants in gas phase: From morphological design to plasmonic enhancement. *Journal of Photochemistry and Photobiology C: Photochemistry Reviews* 24 64–82.

[36] Dionysiou, D. D., Li Puma, G., Ye, J., Schneider, J., Bahnemann, D. (Eds.) (2016). Photocatalysis: Applications. The Royal Society of Chemistry, United Kingdom.

[37] Hanaor, D. A. H., Sorrell, C. C. (2011). Review of the anatase to rutile phase transformation. *Journal of Materials Science* 46 (4) 855–874.

[38] Kumar, S. G., Devi, L. G. (2011). Review on modified TiO_2 photocatalysis under UV/Visible light: Selected results and related mechanisms on interfacial charge carrier transfer dynamics. *The Journal of Physical Chemistry A* 115 (46) 13211–13241.

[39] Carp, O., Huisman, C. L., Reller, A. (2004). Photoinduced reactivity of titanium dioxide. *Progress in Solid State Chemistry* 32 (1) 33–177.

[40] Zhou, K., Zhu, Y., Yang, X., Jiang, X., Li, C. (2011). Preparation of graphene-TiO_2 composites with enhanced photocatalytic activity. *New Journal of Chemistry* 35 (2) 353–359.

[41] Kolasinski, K. W. (2012). Surface science: Foundations of catalysis and nanoscience, 2nd edition. John Wiley & Sons, Ltd., United States of America.

[42] van Gerven, T., Mul, G., Moulijn, J., Stankiewicz, A. (2007). A review of intensification of photocatalytic processes. *Chemical Engineering and Processing: Process Intensification* 46 (9) 781–789.

[43] Wang, W.-Y., Yang, M.-L., Ku, Y. (2010). Photoelectrocatalytic decomposition of dye in aqueous solution using Nafion as an electrolyte. *Chemical Engineering Journal* 165 (1) 273–280.

[44] Wang, N., Li, X., Wang, Y., Quan, X., Chen, G. (2009). Evaluation of bias potential enhanced photocatalytic degradation of 4-chlorophenol with TiO_2 nanotube fabricated by anodic oxidation method. *Chemical Engineering Journal* 146 (1) 30–35.

[45] Khademalrasool, M., Farbod, M., Talebzadeh, M. D. (2016). The improvement of photocatalytic processes: Design of a photoreactor using high-power LEDs. *Journal of Science: Advanced Materials and Devices* 1 (3) 382–387.

[46] Prieto-Rodriguez, L., Miralles-Cuevas, S., Oller, I., Agüera, A., Puma, G. L., Malato, S. (2012). Treatment of emerging contaminants in wastewater treatment plants (WWTP) effluents by solar photocatalysis using low TiO_2 concentrations. *Journal of Hazardous Materials* 211–212 131–137.

[47] da Costa Filho, B. M., Araujo, A. L. P., Silva, G. V, Boaventura, R. A. R., Dias, M. M., Lopes, J. C. B., Vilar, V. J. P. (2017). Intensification of heterogeneous TiO2 photocatalysis using an innovative micro-meso-structured-photoreactor for n-decane oxidation at gas phase. *Chemical Engineering Journal* 310 331–341.

[48] Saquib, M., Muneer, M. (2003). TiO_2-mediated photocatalytic degradation of a triphenylmethane dye (gentian violet), in aqueous suspensions. *Dyes and Pigments* 56 (1) 37–49.

[49] Malato, S., Fernández-Ibáñez, P., Maldonado, M. I., Blanco, J., Gernjak, W. (2009). Decontamination and disinfection of water by solar photocatalysis: Recent overview and trends. *Catalysis Today* 147 (1) 1–59.

[50] Suttiponparnit, K., Jiang, J., Sahu, M., Suvachittanont, S., Charinpanitkul, T., Biswas, P. (2010). Role of surface area, primary particle size, and crystal phase on titanium dioxide

nanoparticle dispersion properties. *Nanoscale Research Letters* 6 (1) 27.

[51] Parrino, F., Camera-Roda, G., Loddo, V., Augugliaro, V., Palmisano, L. (2015). Photocatalytic ozonation: Maximization of the reaction rate and control of undesired by-products. *Applied Catalysis B: Environmental* 178 37–43.

[52] Zhang, X., Zhang, T., Ng, J., Pan, J. H., Sun, D. D. (2010). Transformation of bromine species in TiO_2 photocatalytic system. *Environmental Science & Technology* 44 (1) 439–444.

[53] Tan, T., Beydoun, D., Amal, R. (2003). Effects of organic hole scavengers on the photocatalytic reduction of selenium anions. *Journal of Photochemistry and Photobiology A: Chemistry* 159 (3) 273–280.

[54] Tan, T., Beydoun, D., Amal, R. (2003). Photocatalytic reduction of Se(VI) in aqueous solutions in UV/TiO_2 system: Importance of optimum ratio of reactants on TiO_2 surface. *Journal of Molecular Catalysis A: Chemical* 202 (1–2) 73–85.

[55] Teoh, W. Y., Scott, J. A., Amal, R. (2012). Progress in heterogeneous photocatalysis: From classical radical chemistry to engineering nanomaterials and solar reactors. *The Journal of Physical Chemistry Letters* 3 (5) 629–639.

[56] Adams, M., Skillen, N., McCullagh, C., Robertson, P. K. J. (2013). Development of a doped titania immobilised thin film multi tubular photoreactor. *Applied Catalysis B: Environmental* 130–131 99–105.

[57] Chen, D. H., Ye, X., Li, K. (2005). Oxidation of PCE with a UV LED Photocatalytic Reactor. *Chemical Engineering & Technology* 28 (1) 95–97.

[58] Matsushita, Y., Kumada, S., Wakabayashi, K., Sakeda, K., Ichimura, T. (2006). Photocatalytic reduction in microreactors. *Chemistry Letters* 35 (4) 410–411.

[59] Gorges, R., Meyer, S., Kreisel, G. (2004). Photocatalysis in microreactors. *Journal of Photochemistry and Photobiology A: Chemistry* 167 (2–3) 95–99.

[60] Ghanem, A., Lemenand, T., Della Valle, D., Peerhossaini, H. (2014). Static mixers: Mechanisms, applications, and characterization methods – A review. *Chemical Engineering Research and Design* 92 (2) 205–228.

[61] Li, D., Xiong, K., Yang, Z., Liu, C., Feng, X., Lu, X. (2011). Process intensification of heterogeneous photocatalysis with static mixer: Enhanced mass transfer of reactive species. *Catalysis Today* 175 (1) 322–327.

[62] Díez, A. M., Moreira, F. C., Marinho, B. A., Espíndola, J. C. A., Paulista, L. O., Sanromán, M. A., Pazos, M., Boaventura, R. A. R., Vilar, V. J. P. (2018). A step forward in heterogeneous photocatalysis: Process intensification by using a static mixer as catalyst support. *Chemical Engineering Journal* 343 597–606.

[63] Cathy, M., Nathan, S., Morgan, A., K.J., R. P. (2011). Photocatalytic reactors for environmental remediation: A review. *Journal of Chemical Technology & Biotechnology* 86 (8) 1002–1017.

[64] Colmenares, J. C., Xu, Y.-J. (Eds.) (2016). Heterogeneous photocatalysis: From fundamentals to green applications. Springer-Verlag Berlin Heidelberg, Germany.

[65] Thakur, R. K., Vial, C., Nigam, K. D. P., Nauman, E. B., Djelveh, G. (2003). Static mixers in the process industries - A review. *Chemical Engineering Research and Design* 81 (7) 787–826.

[66] Galaktionov, O. S., Anderson, P. D., Peters, G. W. M., Meijer, H. E. H. (2003). Analysis and optimization of Kenics static mixers. *International Polymer Processing* 18 (2) 138–

150.

[67] Lide, D. R. (Ed.) (2004). Handbook of chemistry and physics. CRC Press, United States of America.

[68] Noguchi, H., Nakajima, A., Watanabe, T., Hashimoto, K. (2002). Removal of bromate ion from water using TiO_2 and alumina-loaded TiO_2 photocatalysts. *Water Science and Technology* 46 (11–12) 27 LP-31.

[69] Noguchi, H., Nakajima, A., Watanabe, T., Hashimoto, K. (2003). Design of a photocatalyst for bromate decomposition: Surface modification of TiO_2 by pseudo-boehmite. *Environmental Science & Technology* 37 (1) 153–157.

[70] Parrino, F., Camera-Roda, G., Loddo, V., Palmisano, G., Augugliaro, V. (2014). Combination of ozonation and photocatalysis for purification of aqueous effluents containing formic acid as probe pollutant and bromide ion. *Water Research* 50 189–199.

[71] Huang, X., Wang, L., Zhou, J., Gao, N. (2014). Photocatalytic decomposition of bromate ion by the UV/P25-Graphene processes. *Water Research* 57 1–7.

[72] Rodriguez, P., Meille, V., Pallier, S., Ali Al Sawah, M. (2009). Deposition and characterisation of TiO_2 coatings on various supports for structured (photo)catalytic reactors. *Applied Catalysis A: General* 360 (2) 154–162.

[73] Moreira, F. C., Soler, J., Alpendurada, M. F., Boaventura, R. A. R., Brillas, E., Vilar, V. J. P. (2016). Tertiary treatment of a municipal wastewater toward pharmaceuticals removal by chemical and electrochemical advanced oxidation processes. *Water Research* 105 251–263.

[74] Denisov, N. M., Baglov, A. V, Borisenko, V. E. (2017). Role of iron and chromium in the photocatalytic activity of titanium dioxide films on stainless steel. *Inorganic Materials* 53 (2) 176–180.

[75] Montecchio, F., Chinungi, D., Lanza, R., Engvall, K. (2017). Surface treatments of metal supports for photocatalysis applications. *Applied Surface Science* 401 283–296.

[76] Pardo, A., Merino, M. C., Coy, A. E., Viejo, F., Arrabal, R., Matykina, E. (2008). Effect of Mo and Mn additions on the corrosion behaviour of AISI 304 and 316 stainless steels in H_2SO_4. *Corrosion Science* 50 (3) 780–794.

[77] Portuguese Goverment (2007). Decreto-Lei n.º 306/2007. *Diário da República n.º 164/2007, Série I de 2007-08-27* 306/2007 5747–5765.

[78] Bak, T., Nowotny, J., Rekas, M., Sorrell, C. C. (2002). Photo-electrochemical hydrogen generation from water using solar energy. Materials-related aspects. *International Journal of Hydrogen Energy* 27 (10) 991–1022.

[79] Ku, Y., Jung, I.-L. (2001). Photocatalytic reduction of Cr(VI) in aqueous solutions by UV irradiation with the presence of titanium dioxide. *Water Research* 35 (1) 135–142.

[80] Nguyen, V. N. H., Amal, R., Beydoun, D. (2003). Effect of formate and methanol on photoreduction/removal of toxic cadmium ions using TiO_2 semiconductor as photocatalyst. *Chemical Engineering Science* 58 (19) 4429–4439.

[81] Marks, R., Yang, T., Westerhoff, P., Doudrick, K. (2016). Comparative analysis of the photocatalytic reduction of drinking water oxoanions using titanium dioxide. *Water Research* 104 11–19.

APPENDIX

APPENDIX A.I – CALCULATIONS FOR STATIC MIXER

Figure A.1 shows the Kenics® SM used and its dimensions.

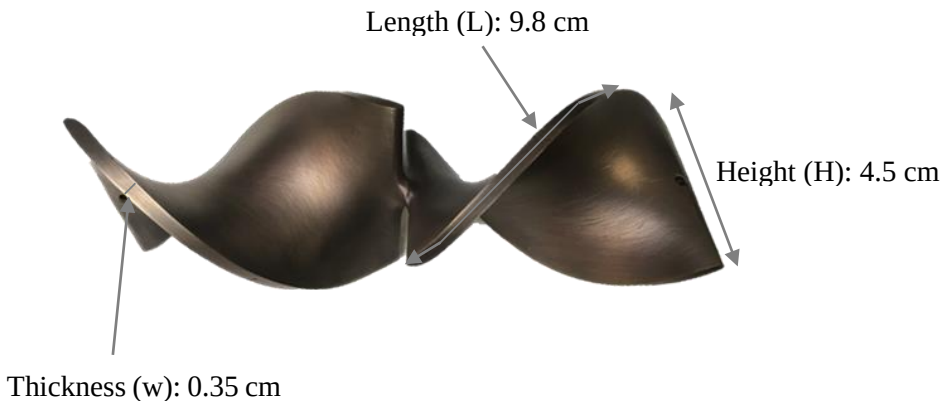

Figure A.1 - Scheme of the SM with its dimensions.

The dimensions presented in the above figure were used to make the following calculations:

$$V_{\text{mixing elements}}\ (\text{cm}^3) = L \times H \times w \times 2 = 9.8 \times 4.5 \times 0.35 \times 2 \cong 31 \quad \text{(A1)}$$

$$\begin{aligned}\text{Total surface area}_{\text{mixing elements}}\ (\text{cm}^2) &= L \times H \times 2 + L \times w \times 2 \\ &= 9.8 \times 4.5 \times 2 + 9.8 \times 0.35 \times 2 \\ &\cong 190\end{aligned} \quad \text{(A2)}$$

$$\begin{aligned}\text{Reactor working volume (L)} &= V_{\text{photoreactor}} - V_{\text{mixing elements}} \\ &= 0.271 - 0.031 \\ &= 0.240\end{aligned} \quad \text{(A3)}$$

$$\begin{aligned}\text{Surface area per unit of reactor volume } (\text{m}^2\ \text{m}^{-3}) &= \frac{\text{Total surface area}_{\text{mixing elements}}}{\text{Reactor working volume}} \\ &= \frac{190 \times 10^{-4}}{0.240 \times 10^{-3}} \\ &\cong 79\end{aligned} \quad \text{(A4)}$$